Unclassified DTIC FILE COPY

SECURITY CLASSIFICATION OF THIS PAGE

REPORT DOCUMENTATION PAGE

AD-A198 421

1b. RESTRICTIVE MARKINGS

3. DISTRIBUTION/AVAILABILITY OF REPORT
Approved for public release; distribution unlimited.

2b. DECLASSIFICATION/DOWNGRADING SCHEDULE

4. PERFORMING ORGANIZATION REPORT NUMBER(S)

5. MONITORING ORGANIZATION REPORT NUMBER(S)
AFOSR-TR. 88-0013

6a. NAME OF PERFORMING ORGANIZATION
University of Illinois at Chicago

6b. OFFICE SYMBOL (If applicable)

7a. NAME OF MONITORING ORGANIZATION
Air Force Office of Scientific Research

6c. ADDRESS (City, State and ZIP Code)
P.O. Box 4348 M/C 273
Chicago, IL 60680

7b. ADDRESS (City, State and ZIP Code)
Electronic and Material Sciences
Bolling Air Force Base, DC 20332-6448

8a. NAME OF FUNDING/SPONSORING ORGANIZATION
Air Force Office of Scientific Research

8b. OFFICE SYMBOL (If applicable)

9. PROCUREMENT INSTRUMENT IDENTIFICATION NUMBER
#F49620-87-C-0021

8c. ADDRESS (City, State and ZIP Code)
Electronic and Material Sciences
Bolling Air Force Base, DC 20332-6448

10. SOURCE OF FUNDING NOS.

PROGRAM ELEMENT NO.	PROJECT NO.	TASK NO.	WORK UNIT NO.
61102F	Darpa		

11. TITLE (Include Security Classification)
Unclassified ("MBE Growth, Characterization..")

12. PERSONAL AUTHOR(S)
Dr. Jean-Pierre Faurie

13a. TYPE OF REPORT	13b. TIME COVERED	14. DATE OF REPORT (Yr., Mo., Day)	15. PAGE COUNT
Semi Annual	FROM 11/13/86 TO 11/12/87	June 30, 1987	21

16. SUPPLEMENTARY NOTATION

17. COSATI CODES		
FIELD	GROUP	SUB. GR.

18. SUBJECT TERMS (Continue on reverse if necessary and identify by block number)

19. ABSTRACT (Continue on reverse if necessary and identify by block number)

Here we report on growth and characterization of high quality HgCdTe grown on CdTe, CdZnTe, CdTeSi and GaAs substrate. A p-type layer grown on a two-inch diameter GaAs (100) substrate exhibiting an excellent uniformity in composition has also been grown.

Extrinsic dopants such as In, As, Sb and Li have been investigated and heterojunctions have been grown in situ.

We report also on the incorporation of mercury in CdTe layers during the growth of HgTe-CdTe superlattices.

DTIC ELECTE AUG 25 1988 E

20. DISTRIBUTION/AVAILABILITY OF ABSTRACT
UNCLASSIFIED/UNLIMITED ☒ SAME AS RPT. ☐ DTIC USERS ☐

21. ABSTRACT SECURITY CLASSIFICATION
Unclassified

22a. NAME OF RESPONSIBLE INDIVIDUAL
Captain Kevin Malloy

22b. TELEPHONE NUMBER (Include Area Code)
(202) 767-4931

22c. OFFICE SYMBOL
NE

DD FORM 1473, 83 APR EDITION OF 1 JAN 73 IS OBSOLETE.

88 8 25 080

Unclassified
SECURITY CLASSIFICATION OF THIS PAGE

MBE GROWTH, CHARACTERIZATION AND ELECTRONIC DEVICE PROCESSING OF HgCdTe, HgZnTe, RELATED HETEROJUNCTIONS AND HgCdTe-CdTe SUPERLATTICES

DARPA - AFOSR - F49620-87-C-0021
November 13, 1986 - November 12, 1989

Semi Annual Technical Report
June 30, 1987

Jean-Pierre Faurie
University of Illinois at Chicago

I. Growth and characterization of high quality HgCdTe

Table I and Table II illustrate the best results obtained for MBE grown n- and p-type layers in terms of carrier concentration and electron or hole mobilities.

Most of these layers have been grown after the starting date of the current contract. An update of these data will be given when appropriate in order to follow the progress that the group is making during the contract. It is important to point out that even if these results are the best ever obtained in the laboratory they are representative of our level of control concerning the growth. Numerous layers with the same composition exhibit very similar results.

A new Hg cell, which is a prototype built by ISA - Riber is currently tested in the laboratory. This cell that we have conceived gives a very stable Hg flux during hours of growth. In table I and II it can be seen that thick layers can be grown using this cell (Sample # 131-318, 2-310, 19405 for example)

Electron mobilities are above 1×10^5 $cm^2V^{-1}s^{-1}$ what is expected for a high quality HgCdTe material with x of about 0.20.

Hole mobilities are very good in the 20% composition and excellent for layers grown on CdTeSe substrate ($\mu h=840$ $cm^2V^{-1}s^{-1}$ for $x=0.31$).

From our result it seems premature to draw a conclusion regarding the choice of the substrate. Electron or hole mobilities are very similar whatever the substrate used to grow HgCdTe.

Table III presents a comparison between (111)B and (100) orientation. Once again, the highest values obtained for electron mobilities are identical for both orientation. However, due to the twinning problem frequently observed in the (111)B, electron mobilities are in average lower for this orientation but, on the other hand, we have demonstrated that the (100) orientation required more mercury than the (111)B orientation.

Most of the layers reported in these tables have a carrier concentration N_a-N_d or N_d-N_a in the mid or low $10^{15}cm^{-3}$ range below 77K.

It should be noted that both mobility and carrier concentration values are suitable for IR device application.

ELECTRICAL CHARACTERISTICS OF HgCdTe MBE P-TYPE LAYERS GROWN BETWEEN 185–195°C.
$(\bar{1}\bar{1}\bar{1})$B ORIENTATION

SAMPLE	SUBSTRATE	COMPOSITION X	THICKNESS e(μm)	T(K)	CARRIER CONCENTRATION $N_A-N_D(cm^{-3})$	MOBILITY $U_H(cm^2v^{-1}s^{-1})$
7434(1981)	CdTe	0.20	5.5	77	$2.0x10^{15}$	660
103 199	CdTe	0.25	8.8	40	$2.6x10^{15}$	550
128 311	CdTe	0.30	7.4	23	$1.0x10^{15}$	360
131 318	CdTe	0.33	12.3	40	$1.7x10^{14}$	240
507 321	GaAs	0.20	4.3	40	$5.9x10^{15}$	840
392 243	GaAs	0.22	1.5	40	$2.2x10^{15}$	520
393 244	GaAs	0.28	1.3	40	$2.8x10^{15}$	520
500 308	GaAs	0.31	2.3	30	$1.1x10^{15}$	450
1-309	CdTeSe	0.31	5.0	30	$2.4x10^{15}$	700
2-310	CdTeSe	0.32	9.4	30	$1.2x10^{15}$	670
4-319	CdTeSe	0.31	7.6	30	$2.4x10^{15}$	840

IMPORTANT: No HgTe layer at the interface

ELECTRICAL CHARACTERISTICS OF HgCdTe MBE N-TYPE LAYERS GROWN BETWEEN 180-190°C x ~ 0.2

SAMPLE	SUBSTRATE ORIENTATION	COMPOSITION X	THICKNESS e(μm)	T	CARRIER CONCENTRATION $N_D-N_A(cm^{13})$	MOBILITY $U_H(cm^2V^{-1}s^{-1}$
7233	CdTe (1981) (111)B	0.20	6.0μm	77K	2×10^{15}	1.9×10^5
11570	CdTe (111)B	0.20	5.0μm	77K	1×10^{16}	1.2×10^5
19405	CdZnTe (111)B	0.20	9.0μm	77K	2×10^{15}	1.2×10^5
576396	GaAs (111)B	0.18	2.7μm	30K	1.5×10^{15}	5.0×10^5
283163	GaAs (111)B	0.20	2.0μm	20K	7×10^{14}	1.2×10^5
191102	GaAs (111)B	0.22	1.0μm	50K	4×10^{15}	1.0×10^5

II. MBE growth and Characterization of two-inch diameter p-type $Hg_{1-x}Cd_xTe$ films on GaAs (100) substrate.

As the Molecular Beam Epitaxial (MBE) growth technique has continued to improve for $Hg_{1-x}Cd_xTe$ films, the prospects for films of larger area have begun to be explored. These larger area films are important for imaging arrays and will be especially vital in the future for the efficient production of $Hg_{1-x}Cd_xTe$ material. The growth by MBE of uniform $Hg_{1-x}Cd_xTe$ epilayer on a large substrate is very difficult to achieve because of the non-uniform distribution of the fluxes and on the non-uniform temperature of the substrate.

But above all, the main problem is due to the exponential change of the Hg condensation coefficient with temperature. We have shown that for a given Hg flux, a high quality monocrystalline $Hg_{1-x}Cd_xTe$ film can be grown in the (111)B orientation within a narrow substrate temperature range (T_{max}-T_{min}) of about 10-15°C if the substrate temperature (T_s) is in the 180-190°C temperature range. When T_s is lower than T_{min} the Hg in excess desorbs but twins, detrimental for the electrical performance, are observed. When T_s is above T_{max} two possibilities exist. If T_s is below 190°C the Te in excess leads to a polycrystalline material. If T_s is above 195°C the excess of Te is reevaporated and the film still grows monocrystalline, but an increase in the x-value of about 1.5 to 2% for each 1°C increase in the substrate temperature is observed along with a large change in the growth rate.

It is important to recall that a change in Δx of only ± 0.001 is the objective suitable to reach for infrared photovoltaic detectors operating with a cutoff wavelength of 10μm at 77K. It is obvious that such a requirement cannot be achieved if part of the substrate is above T_{max}. Now if the substrate temperature is between T_{max} and T_{min} (incidentally T_{max} and T_{min} values are changing over the substrate since the Hg flux distribution is not constant) the epilayers will still experience a change in the doping level and even in the conduction type.

To minimize these temperature variations the rotation of the substrate during the growth can help but a precise temperature measurement of the substrate by a thermocouple is hindered. In order to have an adequate control of the temperature during the growth which can also give reproducible results an infrared pyrometer has been used.

The combination of flux distribution and substrate temperature variation makes the growth by MBE of a large, high quality and uniform $Hg_{1-x}Cd_xTe$ film to be a real challenge.

The film presented here was grown in the (111)B orientation. The film exhibits a uniform mirror-like surface. In order to ascertain the uniformity of this $Hg_{1-x}Cd_xTe$ films over its two-inch diameter surface area, infrared transmission and Van der Pauw D.C. Hall measurements were performed at several positions. The infrared transmission spectra were measured at room temperature. The cutoff wavelengths were in the 6 to 8 μm region. The cutoff wavelength is defined as that for which the absorption coefficient α is equal to 500 cm^{-1}, where the formula for the absorption coefficient is α = -ℓn (transmittance)/thickness. From the measured cutoff wavelengths for each position on the two-inch diameter $Hg_{1-x}Cd_xTe$ films, the Cd concentrations (x) were calculated using Hansen et al.'s relation[7]. Also, from the interference spacing in the infrared transmission spectrum the thicknesses at these positions on the film were determined.

For the p-type film reported here the uniformity of the x-value proved to be excellent, as illustrated in figure 1. The average value of x (denoted by $\bar{x}$) was 0.22, while the standard deviation $\Delta x = [\Sigma(x-\bar{x})^2/n-1]^{1/2}$ was 0.0015, giving as a measure of the composition uniformity $\Delta x/x = 0.7\%$. This is an excellent result since the goal required for IR detectors in terms of composition uniformity is almost achieved on this two-inch diameter $Hg_{1-x}Cd_xTe$ film. This film is entirely p-type. Carrier concentrations (N_a-N_d) and Hall mobilities are reported in Table 1. N_a-N_d increased by a factor of two from 2.6×10^{15} cm^{-3} at the edge of the film, while μ_H increased from 5.7×10^2 $cm^2V^{-1}s^{-1}$ at the center to 6.2×10^2 $cm^2V^{-1}s^{-1}$ at the edge.

These variations are supposed to be due to a non uniform flux distribution and a non uniform substrate temperature. A ΔT_s of about 5°C has been measured over 2 inches.

This result represents an important achievement for the future of IR detectors. As an important comparison this result is as good as those reported for OMCVD HgCdTe films grown on a surface area of only [x]cm^2.

$Hg_{1-x}Cd_xTe$ (111)B grown on 2° GaAs(100)–Sample #583453

T_s = 195 °C

Thickness = 5.4 μm

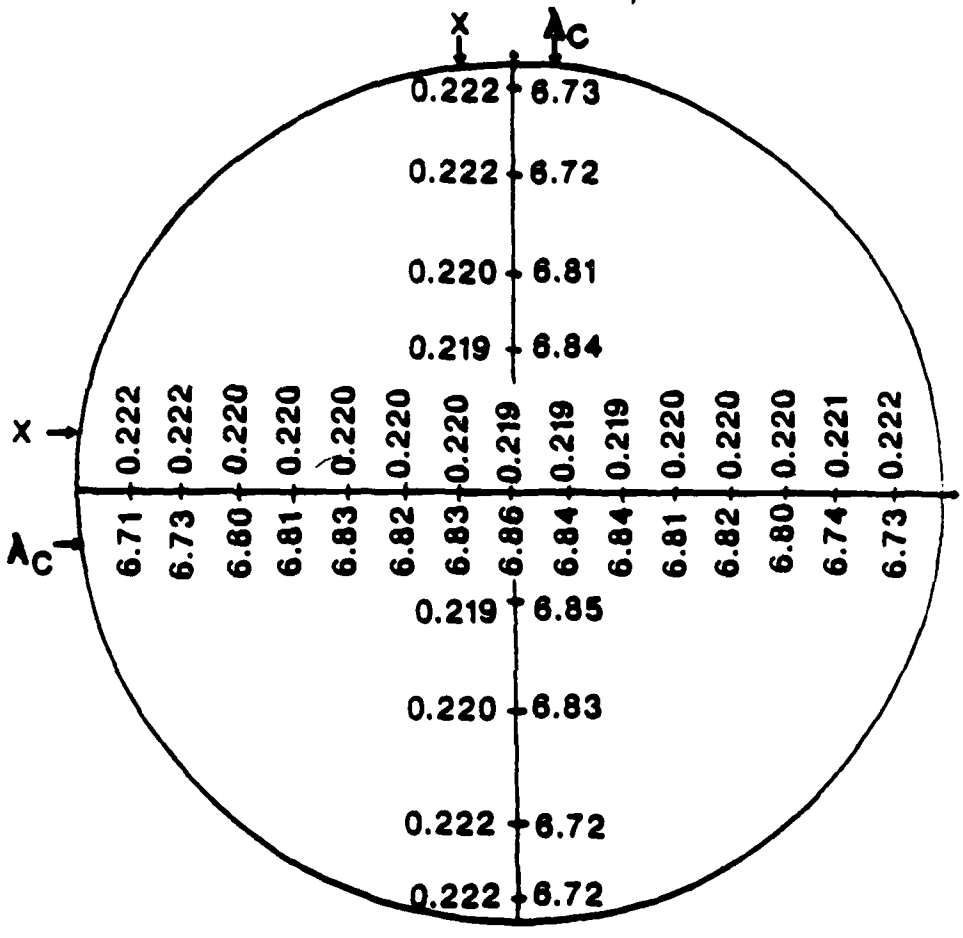

λ = cut-off wavelength in μm at 300K

$\bar{x}$ = 0.22 $\qquad$ $\bar{\lambda}$ = 6.78 μm

$\Delta x_{SD} = \sqrt{\frac{\Sigma(x-\bar{x})^2}{n-1}} = 0.0015$ $\qquad$ $\Delta\lambda_{SD}$ = 0.08 μm

$\frac{\Delta x_{SD}}{\bar{x}}$ = 0.7 %

Table I – Hall measurements at B = 0.2 Tesla for two-inch diameter $Hg_{1-x}Cd_xTe$(111) film grown at 190°C on CdTe(111)/GaAs(100) substrate. Sample #583453.x=0, y=0 is at the center of the sample.

x (mm)	y (mm)	Cond. Type	300K N_d-N_a (cm^{-3})	μ_H ($cm^2V^{-1}s^{-1}$)	T(K) when $R_H=0$	Cond. Type	40K N_a-N_d (cm^{-3})	μ_H ($cm^2V^{-1}s^{-1}$)
0	0	n	2.1×10^{16}	6.4×10^{3}	90	p	3.6×10^{15}	5.7×10^{2}
4	0	n	2.0×10^{16}	5.0×10^{3}	90	p	3.0×10^{15}	5.2×10^{2}
7	0	n	2.1×10^{16}	6.3×10^{3}	90	p	4.7×10^{15}	5.5×10^{2}
11	0	n	1.9×10^{16}	6.2×10^{3}	90	p	5.1×10^{15}	5.7×10^{2}
15	0	n	1.9×10^{16}	6.8×10^{3}	90	p	5.6×10^{15}	6.5×10^{2}
18	0	n	1.8×10^{16}	6.8×10^{3}	90	p	7.2×10^{15}	6.2×10^{2}
0	7	n	1.9×10^{16}	6.6×10^{3}	90	p	4.9×10^{15}	6.0×10^{2}
0	15	n	1.8×10^{16}	6.8×10^{3}	90	p	6.1×10^{15}	6.7×10^{2}

III. Doping

N-Type

We have shown in the previous DARPA contract (MDA 903-83K-0251) that indium can be incorporated as an active impurity with a high electrical efficiency in HgCdTe layers during the MBE growth.

Indium is a very good n-type dopant:

(1) it has a high electrical efficiency (70 to 100%) and that without any activation (see fig. 1);
(2) high doping levels up to $10^{19}cm^{-3}$ have been reached;
(3) high electron mobility of $1\times10^{5}cm^{2}V^{-1}s^{-1}$ have been observed for doping level of $2\times10^{16}cm^{-3}$;
(4) abrupt junctions can be grown (see fig. 1).

But indium presents a serious problem. Memory effect has been observed which means that some residual indium (10^{15} - $10^{16}cm^{-3}$ range) is found in epilayers grown after In-doped epilayers have been grown. This effect is supposed to be due to indium-tellurium chemical reaction(s) taking place in different parts of the MBE chamber. The compound(s) can later be reevaporated and dissociated if they are heated. Te, In and CdTe effusion cells have been found to be the sources of contamination along with the walls surrounding the effusion cells and the substrate heater.

This problem has been worked out for months but no satisfactory solution has been found, therefore another n-type dopant has to be investigated.

P-type

Arsenic and Antimony

Group V elements can be incorporated into HgCdTe as acceptors in substitution of non-metal lattice sites using the liquid phase epitaxy. However, group V elements have not been successfully incorporated into MBE grown HgCdTe layer as acceptors. Both Sb and As have been tried and they behave as n-type dopants as

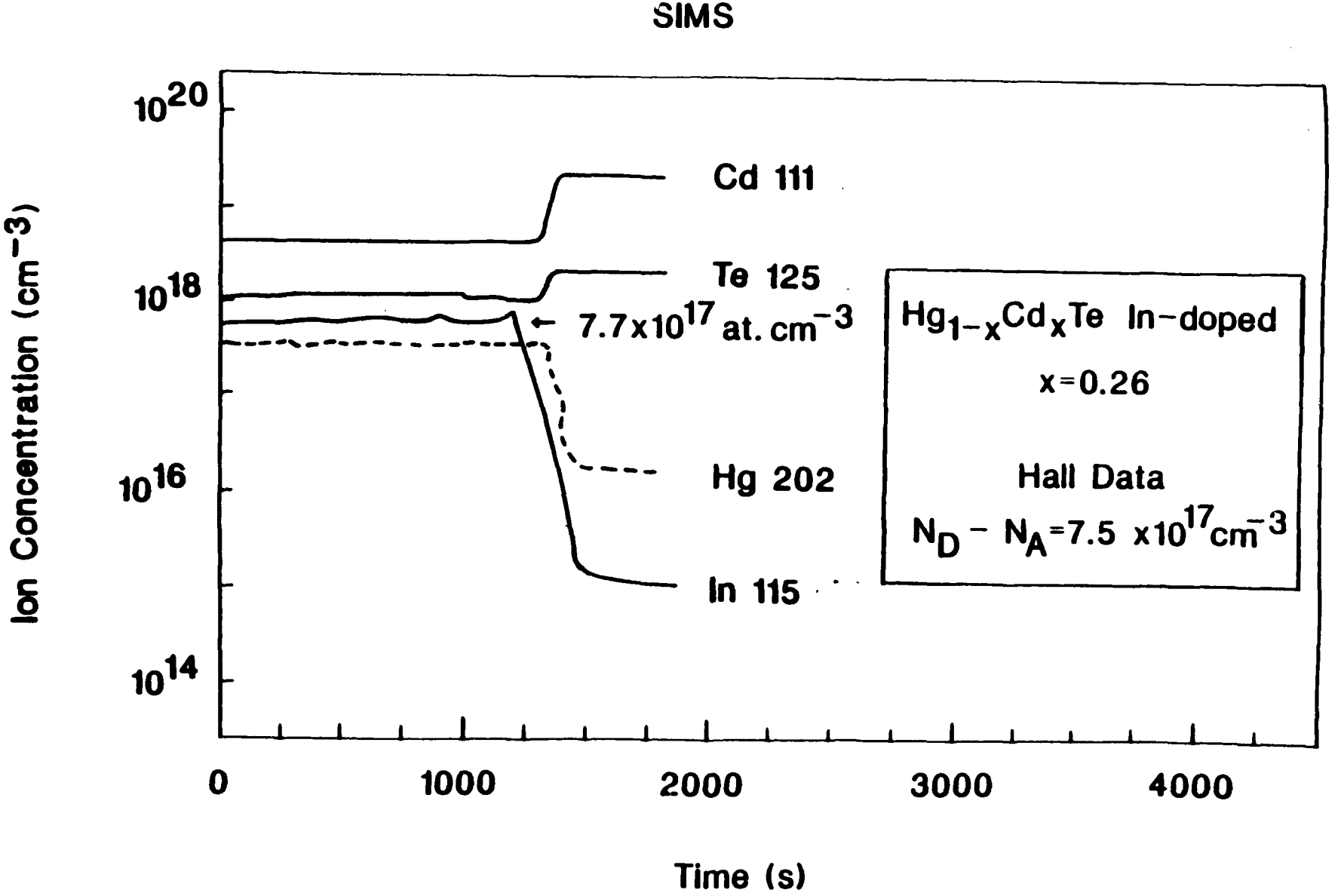
SIMS
Ion Concentration (cm^{-3})
10^{20}
10^{18}
10^{16}
10^{14}
Cd 111
Te 125
7.7×10^{17} at. cm^{-3}
Hg 202
In 115
$Hg_{1-x}Cd_xTe$ In-doped
x=0.26
Hall Data
$N_D - N_A = 7.5 \times 10^{17} cm^{-3}$
0
1000
2000
3000
4000
Time (s)

illustrated in Table IV and Table V.

A cracker cell has been used for As and Sb which means that the flux was constituted by As_4 + As_2 molecules or by Sb_4 + Sb_2 molecules.

Some of the As doped HgCdTe layers were annealed using the close tube method. For these annealing a drop of Hg was used to control the Hg pressure and the Hg temperature was kept higher than the sample temperature. Table IV shows the electrical measurements of two As doped HgCdTe layers before and after annealing.

The annealing increases the As electrical activity as a donor, and not as an acceptor, by a factor of 4 to 5.

Sample #508331 and 511334 which have been grown with the same As cell temperature have about the same SIMS counts. But sample #511334 has a higher carrier concentration (factor 2 to 3) both before and after annealing. Sample #511334 was exposed to UV light while growing and not sample #508331.

Thus it appears that when exposed to UV light the electrical activity of As in HgCdTe increases as a *n*-type dopant.

This is not completely surprising if we consider that As is incorporated as a n-type dopant because As-Te bonds are established in preference to As-Hg or As-Cd. UV light is supposed to break Te_2 molecule (E~3eV) making Te even more reactive with As.

These experiments do not conclude that As or Sb cannot be incorporated as p-type dopants in MBE grown layers. SIMS analysis shows that only a few percent of As or Sb are electrically active. In fact, if one considers the heat of formation ΔH_f of some tellurides it appears that ΔH_f for Sb_2Te is equal to -4.5 kcal/mole, less than ΔH_f of HgTe (-7.6 kcal/mole). No data have been found for As_2Te but ΔH_f should not be very different. This means that Sb_2Te and As_2Te are more unstable than HgTe itself. It is unclear yet how As or Sb are acting as donors incorporated in Hg vacancies or in interstitial sites. But it seems very likely that they could be incorporated as acceptors. A higher Hg flux, light, electron or ion beams have to be investigated.

As-doped HgCdTe ($\overline{111}$)B MBE layers

Sample	x	TAs cell(c)	T_{HALL}(K)	as-grown cc(cm^{-3})	as-grown μ_H($cm^2V^{-1}s^{-1}$)	After annealing cc	After annealing μ_H
133 329	0.22	230	77	n-2.5×10^{16}	7.0×10^3		
8 326	0.22	0	30	p-1.8×10^{16}	600		
508 331	0.28	250	77	n-2.5×10^{15}	5.0×10^3	n-1.5×10^{16}	4.3×10^4
511 334 (UV light)	0.29	250	77	n-8.0×10^{15}	4.5×10^3	n-3.8×10^{16}	2.3×10^4
509 332	0.29	0	30	p-3.0×10^{15}	260		

Sb-doped HgCdTe $(\overline{1}\overline{1}\overline{1})$B MBE layers

Sample	X	$T_{Sb\ cell}$(c)	Orientation	CC(cm^{-3})	μm($cm^2V^{-1}s^{-1}$)
547 369	0.20	450	(111)	n-8 x 10^{15}	2 x 10^4
551 370	0.20	0	(111)	p-8 x 10^{15}	300
546 368	0.23	350	(111)	n-1 x 10^{15}	1 x 10^4
545 367	0.24	0	(111)	p-2.5 x 10^{16}	600
562 378	0.26	500	(111)	n-2.6 x 10^{15}	9 x 10^3

Lithium

It has been shown that under regular MBE growth conditions As and Sb are incorporated as donors in HgCdTe. Therefore in order to obtain p-type HgCdTe layers incorporation of a Group I element was studied.

Lithium was the first element investigated. It is found that Li is indeed incorporated as an acceptor. Acceptor concentrations as high as $8\times10^{18}cm^{-3}$ have been achieved. An incorporation coefficient of Li close to one and almost a 100% electrical efficiency for Li were observed in Li-doped $Hg_{1-x}Cd_xTe$ epilayers grown by MBE without any external activation. However, Li is found to diffuse rapidly in MBE HgCdTe grown layers.

For more detail see the attached paper entitled "Electrical Properties of Li Doped $Hg_{1-x}Cd_xTe(100)$ by Molecular Beam Epitaxy" which will appear in Applied Physics Letters in December 1987.

IV. $Hg_{1-x}Cd_xTe/Hg_{1-y}Cd_yTe$ Heterojunctions Grown in Situ by MBE

Isotype n-N abrupt heterojunctions where grown in situ by MBE on CdTe(-111)//GaAs(100) combination substrates. The first devices tested had x = .18 on the bottom and x = .26 on the top. All the electrical and optical characterizations were consistent with the presence of narrow and strong composition burst right at the interface. The R_oA was limited by the wide-gap side (see attached publication entitled "Mercury Cadmium Telluride n-Isotype Heterojunctions Grown in Situ by Molecular Beam Epitaxy."

The later devices grown with care to avoid the problem had drastically different behavior. The compositions where slightly higher on both sides: x = .22 for the bottom and .28 for the top. Strong rectification was seen with quality factors varying from 2 at high temperatures to 2.5 at 80K (fig. 2). The forward bias occurred when the top material was biased negatively. One device had an R_oA as high as $10^4\ \Omega cm^2$ at 80K, but this value was only seen once. In the average it typically reaches 10^3 at 80K (fig. 3). The activation energy of I_s/T^2 varies from .1eV at high temperature to .06eV at 80K (fig. 4). the spectral response shows a maximum at 8μm wavelength, without sharp peak at short wavelength as before (fig. 5). The capacitance measurements are unreliable since the top material thickness was as small as .5μm, and the top contact is

suspected to have a smaller area than expected. A low current density $10^{-2}A/cm^2$ can blow the devices opened. These measurements are consistent with a Schottky type behavior at the heterojunction, most of the depletion occurring in the wide bandgap material, which is limiting the R_oA. Thermionic emission is not the only process involved in the transport since the quality factor is higher than 2. This renders the barrier height determination unreliable, even if it seems consistent with the expected bandgap difference between the two sides.

HETEROJUNCTION

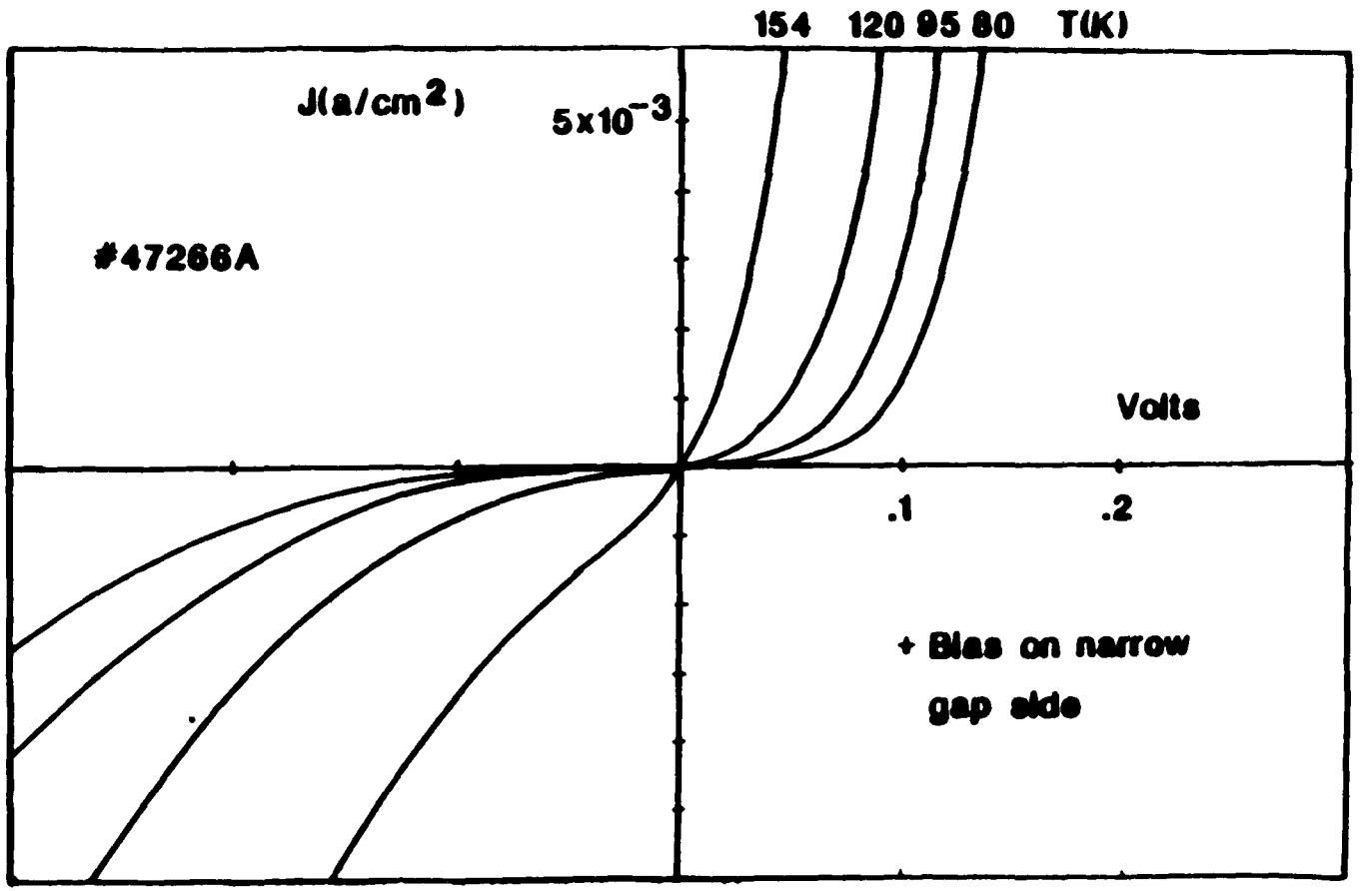

Current Voltage Curves

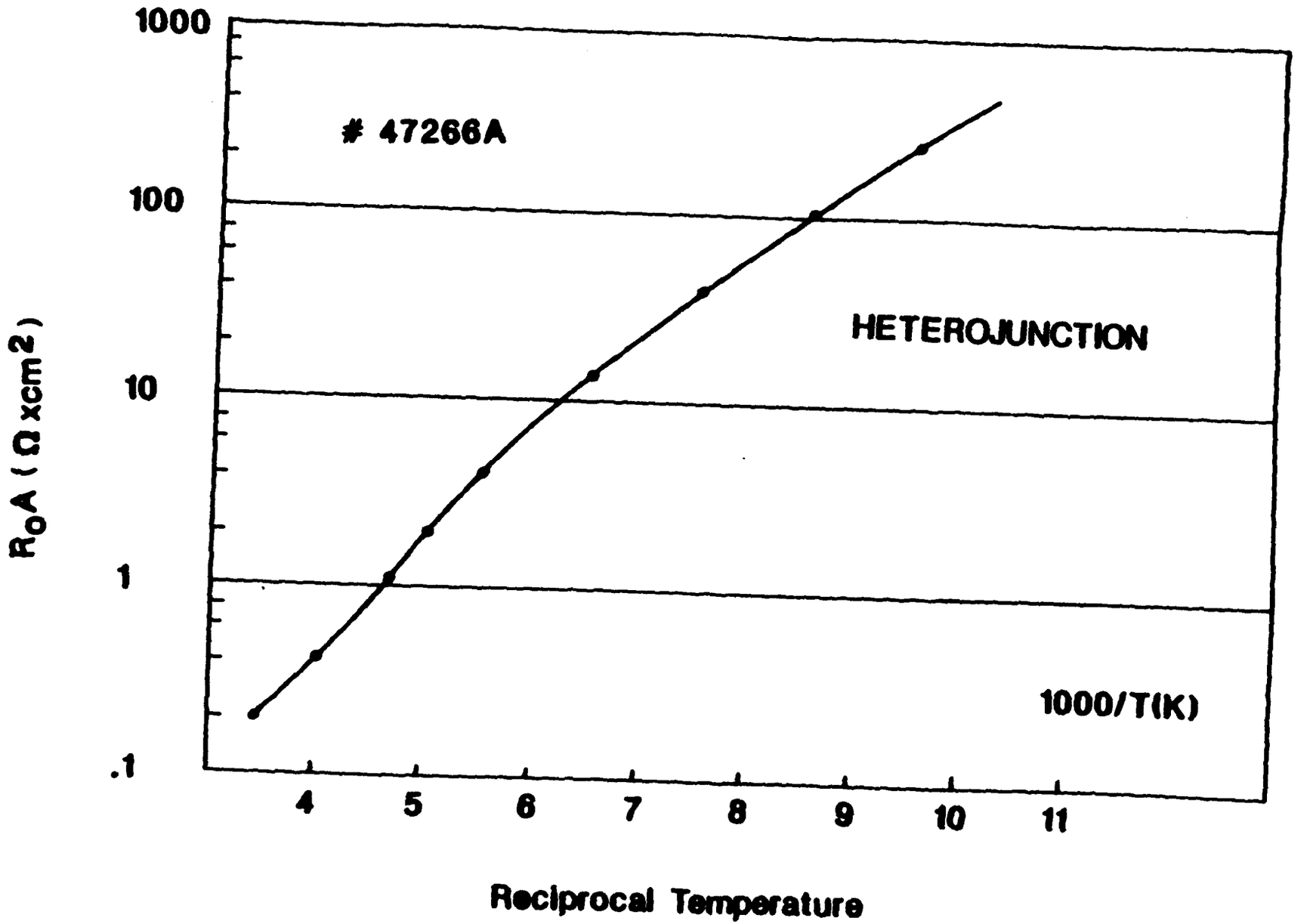
1000
100
10
1
.1
47266A
HETEROJUNCTION
1000/T(K)
4
5
6
7
8
9
10
11
R_oA (Ω xcm^2)
Reciprocal Temperature

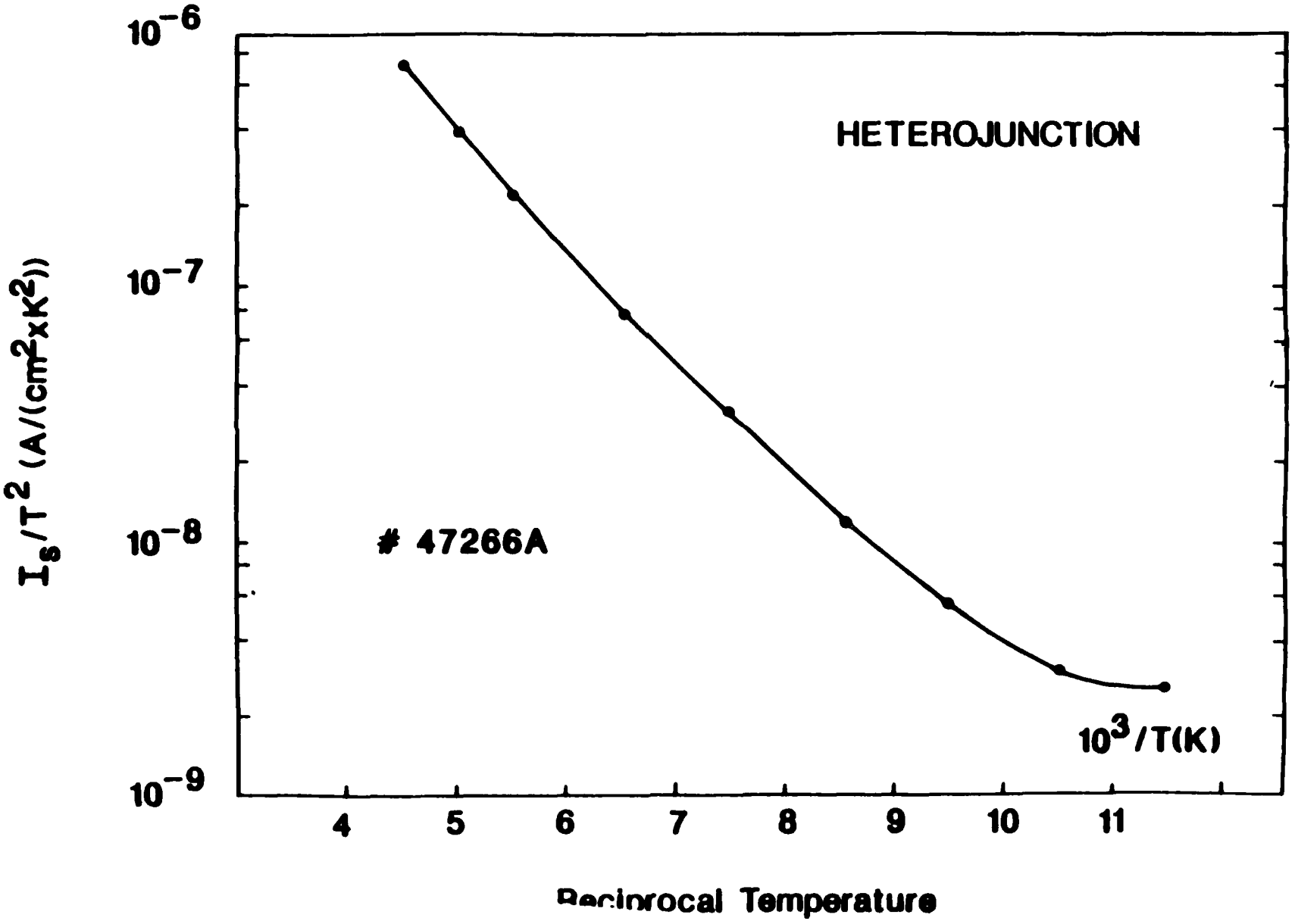
HETEROJUNCTION
47266A
10^{-6}
10^{-7}
10^{-8}
10^{-9}
I_s/T^2 (A/(cm^{2}xK^2))
4
5
6
7
8
9
10
11
10^3/T(K)
Reciprocal Temperature

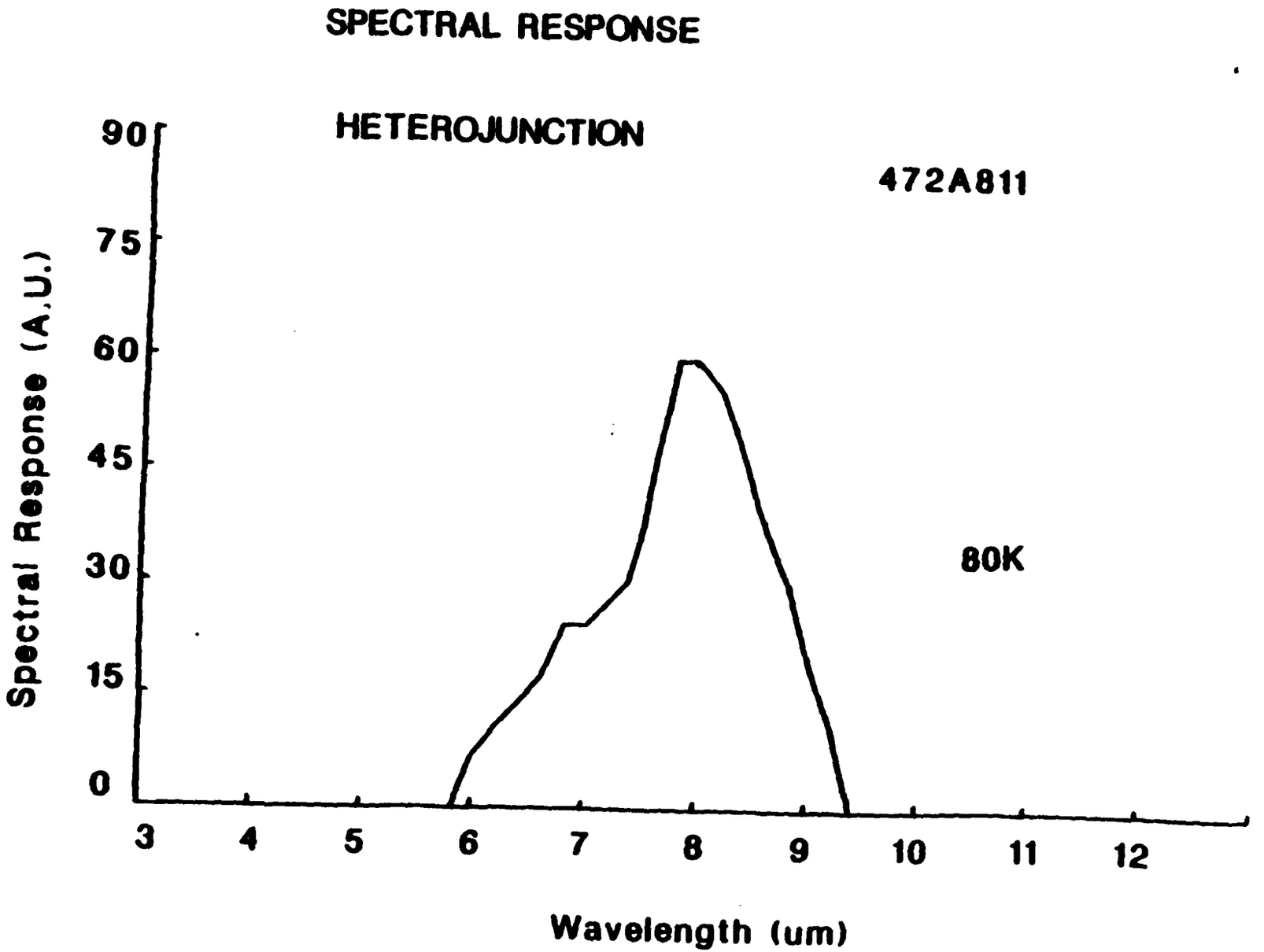
SPECTRAL RESPONSE
HETEROJUNCTION
472A811
80K
Spectral Response (A.U.)
90
75
60
45
30
15
0
3
4
5
6
7
8
9
10
11
12
Wavelength (um)

V. HgTe-CdTe Superlattices: Hg incorporation in CdTe layers during MBE growth

It was shown in 1982 that HgTe-CdTe superlattices (SLs) could be grown by MBE. But due to the noncongruent evaporation of Hg from HgTe, the Hg flux must be maintained even during the growth of the CdTe layers. This means that some Hg is incorporated in the CdTe during its growth. There are two important questions that arise. First, how will this Hg incorporation affect the bandgap of the SL. Second, how much Hg is in the CdTe.

We determine the period of the SL by the position of the X-ray satellite peaks. The average Hg composition in the SL is then measured by EDS. The period and the average Hg composition are then used to compute the individual layer thicknesses if the percentage of Hg in the CdTe is known. Using this method, for the same period and average Hg composition, as the amount of Hg in the CdTe increases several things will occur. First, the thickness of the HgTe layers will decrease. This will tend to increase the bandgap. Second, the CdTe will become $Hg_xCd_{1-x}Te$ with a smaller bandgap. This decrease in the barrier height will tend to decrease the SL bandgap. Finally, the width of the $Hg_xCd_{1-x}Te$ will increase. This will have a small tendency to increase the bandgap. The total effect on the SL bandgap of all these changes would be small.

We have grown, with a Hg flux, thick layers of CdTe under the same conditions as in our SLs [190 to 200°C on (111)B]. The amount of Hg measured in the layer by EDS was less than 5%. On a series of thin CdTe (111)B layers grown under a Hg flux the amount of Hg was carefully measured by XPS. This is done using both the ratio of the peak areas and the difference in energy between the core level and valence band maximum. For the growth conditions that we actually use in our SLs, these results agree with those obtained for the thick layers. The Hg incorporation varies, up to 9%, depending on the growth conditions. This should only slightly affect the characteristics of the HgTe-CdTe SLs and other microstructures, such as single and double barrier tunneling structures.

These results indicate that some Hg is incorporated in the CdTe but that under our normal conditions this amount is small. The Hg incorporation is crystal orientation dependent. For the (100) surfaces, about 15% Hg are observed for growth conditions identical to those used for the (111).

For more information see the attached paper accepted for publication in Applied Physics Letters (Nov. 1987) entitled "Hg Incorporation in CdTe During the

Growth of HgTe-CdTe Superlattices by Molecular Beam Epitaxy."

VI. A review paper on Hg-based, microstructures is attached here. Most of the results presented in this paper have been obtained under DARPA sponsorship.

Electrical properties of Li-doped $Hg_{1-x}Cd_xTe(100)$ by molecular beam epitaxy

P. S. Wijewarnasuriya, I. K. Sou, Y. J. Kim, K. K. Mahavadi, S. Sivananthan, M. Boukerche, and J. P. Faurie
Department of Physics, University of Illinois at Chicago, Chicago, Illinois 60680

(Received 1 July 1987; accepted for publication 12 October 1987)

p-type doping of HgCdTe(100) layers with lithium during growth by molecular beam epitaxy is reported. Hall measurements have been performed on these layers between 300 and 30 K. The Li concentration is found to increase with the Li cell temperature. Li-doped HgCdTe layers are estimated to have very shallow acceptor levels. Acceptor concentrations as high as 8×10^{18} cm^{-3} have been achieved. At low doping levels, due to residual donors, layers show compensation. Incorporation coefficient of Li close to 1 and almost 100% electrical efficiency for Li in molecular beam epitaxy HgCdTe layers were observed. However, Li is found to diffuse rapidly in HgCdTe layers grown by molecular beam epitaxy.

Over the past ten years $Hg_{1-x}Cd_xTe$(MCT) has emerged as an important material for infrared (IR) detector technology. MCT was grown by molecular beam epitaxy (MBE) on CdTe substrates for the first time in 1981.[1] Since then, this technique has produced MCT layers of either *n* or *p* type and of a quality comparable to the layers grown by other techniques. However, very little information exists on the incorporation of foreign elements in MBE grown epitaxial layers. Recently, successful *n*-type doping of MCT layers with indium during growth by MBE was reported.[2] Carrier concentrations of two orders of magnitude more than what can be achieved by stoichiometry deviation have been reached for MBE layers grown in the (111)*B* orientation. Antimony and arsenic (group V elements) act as *p*-type dopants in MCT using other growth techniques[3] such as liquid phase epitaxy. But in the case of MBE grown MCT layers, both Sb and As behave as *n*-type dopants.[4] In the case of (100) orientation only *n*-type MCT with doping levels ranging from 10^{15} to mid-10^{16} cm^{-3} can easily be produced by stoichiometry deviation for $x<0.35$. *p*-type (100) is difficult to achieve for $x<0.24$.[5] Therefore, in order to obtain *p*-type MCT layers in the (100) orientation, incorporation of foreign elements in group I was studied. Li behaves as a *p*-type dopant, as expected. Here, we report results on Li, the first impurity successfully incorporated as an electrically active acceptor in MBE grown MCT layers.[4] In this letter, we present electrical properties of lithium-doped MCT(100) MBE layers studied by variable temperature Hall measurements.

MCT layers were grown in a Riber 2300 MBE machine which is designed to handle mercury. MCT layers were grown on 2–3 μm thick CdTe buffer layers which were deposited on GaAs(100) substrates. The growth was monitored by reflection high-energy electron diffraction (RHEED). The growth rate was 4–5 Å/s. Li was provided by a separated effusion cell loaded with pure Li. Since it is a very reactive material, great care has been taken when loading it into the growth chamber. This was done in an inert atmosphere. The Li cell temperature range was 205–280 °C. The Cd composition in the MCT layers was determined at room temperature by infrared transmission measurements and by energy dispersive spectroscopy measurements. The secondary ion mass spectroscopy (SIMS) technique was used to obtain the concentration profile of Li atoms through the layers. Since we did not have a standard sample containing Li, we were not able to relate the number of counts from the SIMS to the actual Li concentration. Therefore, all SIMS data are given in arbitrary units, but a relative comparison is significant. The carrier concentration and the Hall mobility in the layers were evaluated by the Van der Pauw technique[6] between room temperature and 30 K. A $AuCl_3$ solution was used to form ohmic contacts, and the ohmicity of the contacts was checked systematically. A magnetic field strength of 2000 G was used for the Hall measurements.

Electrical measurements of the Li-doped MCT layers at 40 K are summarized in Table I. Figure 1 shows the variation of the carrier concentration (deduced from the Hall coefficient) versus $1000/T$(K) for three samples. A typical freeze-out behavior cannot be seen for the larger doping levels. This happens even with mid 10^{17} doping levels and above. Such an effect has been reported previously for phosphorus.[7] Furthermore, it can be seen from the figure that the mixed conduction $n\rightarrow p$ transition region diminishes when the doping level increases. For the higher doping levels, the carrier concentration is independent of temperature, indicating that electrically active acceptors are completely ionized. The total amount of electrically active Li concentration in the samples was determined from the low-temperature carrier concentration data.

The only layer (sample No. 1) which shows the freeze-out behavior has been analyzed numerically[8] using the charge neutrality equation:

$$n+N_a^{-}=p+N_d^{+},$$

where n, p, N_d^{+}, and N_a^{-} are the concentration of electrons, holes, ionized donors, and ionized acceptors, respectively. For the donors, complete ionization is assumed and the concentration of ionized acceptors is given by

$$N_a^{-}=\frac{N_a}{1+4\times\exp(x_a-\eta_f)},$$

where x_a is the reduced acceptor level with respect to valence band and η_f is the reduced Fermi level.

 0003-6951/87/502025-03$01.00

TABLE I. Electrical measurements of lithium-doped MCT at 40 K. Samples No. 6 and No. 7 represent n-type MBE grown MCT(100).

Sample No.	Thickness (μm)	Cd composition (%)	$N_a - N_d$ ($\times 10^{16}$ cm^{-3})	Mobility at 40 K (cm^2/V s)	Li cell temp. (°C)
1	1.68	25	+ 0.84	370	205
2	1.38	17	+ 52.00	360	219
3	2.16	20	+ 200.00	330	245
4	2.18	23	+ 800.00	330	282
5	1.92	21	+ 440.00	340	270
6	1.00	20	− 1.00	3.0×10^3	···
7	6.20	19	− 1.00	2.4×10^3	···

From the Kane model[9] for nonparabolic bands,

$$n = \frac{K_B T}{2\pi^2}\left(\frac{3}{2P^2}\right)^{3/2}\int_0^{+\infty}\frac{x^{1/2}(x+x_g)^{1/2}(2x+x_g)}{1+\exp(x+x_g-\eta_f)}\,dx,$$

where P is the momentum matrix element of the Kane model and x_g is the reduced energy gap. For the band gap E_g, an empirical equation is used from Ref. 10. Since the equilibrium concentration of light hole is negligible, p is the heavy-hole concentration. Parabolic band with Fermi–Dirac statistics is assumed for the heavy holes. Since the mixed conduction dominates at high temperature, the concentration is deduced from the following equation:

$$\text{c.c.} = (p + nb)^2/(p - nb^2),$$

where b is the ratio of electron-to-hole mobility and is given by

$$b = \mu_e/\mu_h = \tau\, m_h^*/m_e^*,$$

where $m_e^* = 3\hbar^2 E_g/4P^2$, $m_h^* = 0.63m_e$,[11] and $P = 8\times10^{-8}$ eV cm.[11] When calculating, N_a, N_d, τ, and E_a were adjusted to give the best fit for the experimental carrier concentration data. The solid line in Fig. 1 is the best fit. It was obtained with $N_a = 1.89\times10^{16}$ cm^{-3}, $N_d = 1.05\times10^{16}$ cm^{-3}, $\tau = 0.24$, $E_a = 8.3$ meV, and Cd composition = 25.8%.

Figure 2 shows mobility versus doping concentration at 40 K. It can be seen that the hole mobility in the Li-doped samples at 40 K does not vary drastically with the hole concentration. Doping levels as high as 8×10^{16} cm^{-3} were achieved. At low doping levels, experimental results indicate a large degree of compensation in the layers, since along the (100) growth orientation, only n-type MBE grown MCT(100) layers are currently achieved by stoichiometry adjustment (see Table I). This large degree of compensation accounts for the limitation of the hole mobility at low doping levels.

Figure 3 shows the concentration of Li atoms in the MCT layers calculated from the incident flux and from growth rate (assuming unity sticking coefficient) versus $1000/T$(K), where T is the Li cell temperature. The carrier concentration $N_a - N_d$ (extracted from Hall measurements) and the SIMS Li counts are also plotted in Fig. 3. By comparing the concentration of electrically active Li atoms in the layers from Hall measurements and the concentration of Li atoms incorporated into layers calculated from the incident flux, it can be seen that there is good agreement within the experimental error. At this range of doping levels, $N_a - N_d$ extracted from Hall measurements is approximately equal to the acceptor concentration N_a, since residual donor concentration is of the order of 10^{16} cm^{-3}. Therefore, this agreement is an indication that almost 100% of the Li is electrically efficient, and also that the incorporation of Li in MBE grown MCT layers is close to 1. As can be seen from Fig. 3, the SIMS data fall on a straight line, indicating that the number of Li atoms incorporated into the samples de-

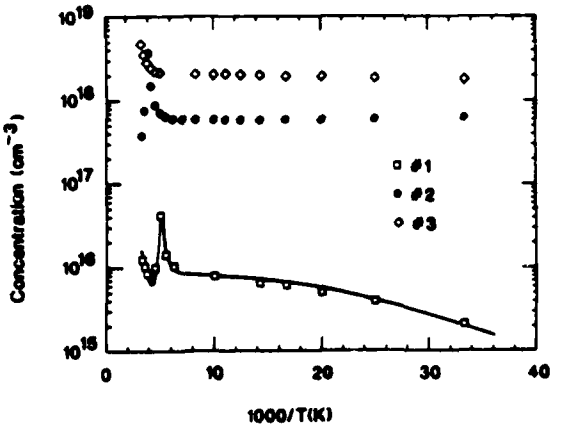

FIG. 1. Hole concentration as a function of $1000/T$(K) for lithium-doped MCT layers grown by MBE. The solid line for sample No. 1 is the best fit obtained for the following parameters: $N_a = 1.89\times10^{16}$ cm^{-3}, $N_d = 1.05\times10^{16}$ cm^{-3}, $\tau = 0.24$, and $E_a = 8.3$ meV.

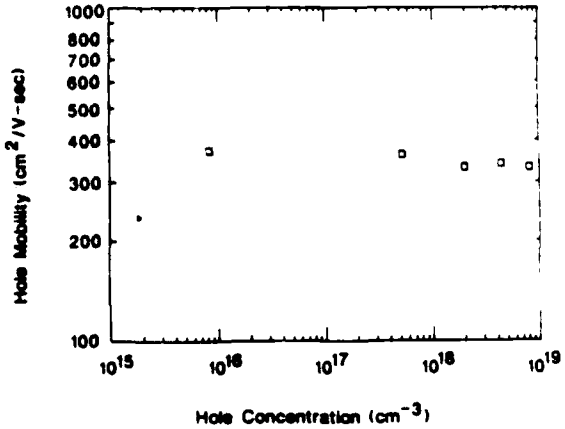

FIG. 2. Experimental hole mobility at 40 K as a function of the hole concentration for lithium-doped MCT layers.

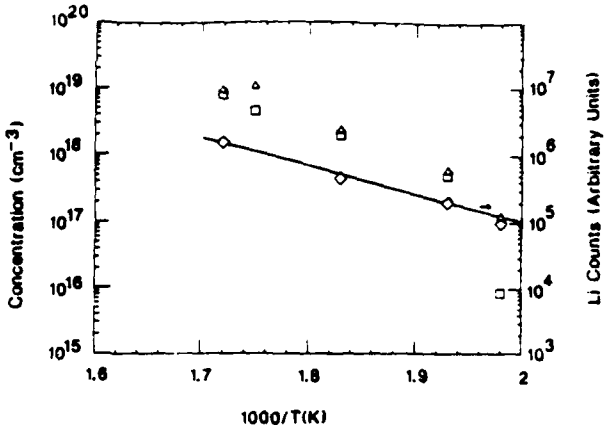

FIG. 3. Li counts (◇) obtained by SIMS in the layers, $N_a - N_d$ (cm^{-3}) from Hall measurements (□) and Li concentration (cm^{-3}) calculated from the incident flux (△) vs reciprocal of the Li cell temperature.

creases exponentially with the reciprocal of the Li cell temperature. Sample No. 1, which has the lowest Li cell temperature, exhibits a large discrepancy between Li concentration as calculated from the incident flux and as measured from Hall measurements. This discrepancy is due to the compensation in the layers because the level of electrically active impurities(Li) is not much larger than the intrinsic donors.

In order to investigate the diffusivity of Li, a sample consisting of a nondoped MCT layer (0.93 μm thick) on top of a Li-doped MCT layer (0.93 μm thick) has been grown. From the SIMS profile of this sample, Li can be seen in the undoped layer in amounts comparable to that in the intentionally doped one. This indicates that Li is highly mobile in MCT layers grown by MBE. At this point, we have no evidence from SIMS data that Li is diffusing in CdTe buffer layer and substrate.

In conclusion, we have demonstrated that Li behaves as a p-type dopant in MBE grown $Hg_{1-x}Cd_xTe(100)$. This represents the first successful attempt to incorporate electrically active acceptors during MBE growth. These Li-doped MCT layers have been estimated to have very shallow acceptor levels for sample No. 1, which showed the freeze-out. The calculated activation energy was 8.3 meV. Using Li as a p-type dopant, carrier concentrations up to 8×10^{18} cm^{-3} have been achieved. At low doping levels, layers show compensation due to the residual donors from stoichiometry deviation. The doping level in the samples can be controlled by varying the Li cell temperature. An incorporation coefficient of 1 and almost 100% electrical efficiency for Li in MBE grown MCT layers were observed. However, the SIMS profile indicates that Li is highly mobile in MCT layers. This represents a limitation in the use of this element, especially for abrupt heterojunctions.

We wish to acknowledge G. Monfroy for performing the energy dispersive spectroscopy measurements for some of the samples, and Z. Ali and A. Farook for their technical assistance. This work was funded by the Defense Advanced Research Project Agency and monitored by the Air Force Office for Scientific Research under contract No. F49620-87-C-0021

[1] J. P. Faurie and A. Million, J. Cryst. Growth 54, 582 (1981).
[2] M. Boukerche, J. Reno, I. K. Sou, C. Hsu, and J. P. Faurie, Appl. Phys. Lett. 48, 1733 (1986).
[3] P. Capper, J. Cryst. Growth 57, 280 (1982).
[4] J. P. Faurie, DARPA II- VI Materials & Processing Conference, Washington, April 1987 (unpublished results)
[5] J. M. Arias, S. H. Shin, J. T. Chen, S. Sivananthan, J. Reno, and J. P. Faurie, J. Vac. Sci. Technol. A 5, 3133 (1987).
[6] L. J. van der Pauw, Philips Tech. Rev. 20, 220 (1958).
[7] H. R. Vydyanth, R. C. Abbot, and D. A. Nelson, J. Appl. Phys. 54, 1323 (1983).
[8] M. Boukerche, P. S. Wijewarnasuriya, J. Reno, I. K. Sou, and J. P. Faurie, J. Vac. Sci. Technol. A 4,2072 (1986).
[9] E. O. Kane, J. Phys. Chem. Solids 1, 249 (1957).
[10] E. Finkman and S. E. Schacham, J. Appl. Phys. 56, 2896 (1984).
[11] E. Finkman, J. Appl. Phys. 54, 1883 (1983).

Mercury cadmium telluride *n*-isotype heterojunctions grown *in situ* by molecular-beam epitaxy

M. Boukerche, I. K. Sou, M. DeSouza, S. S. Yoo, and J. P. Faurie
Department of Physics, University of Illinois at Chicago, Chicago, Illinois 60680

(Received 10 November 1986; accepted 7 May 1987)

Electrical characterizations of the first *n–N* HgCdTe heterojunctions grown *in situ* by molecular-beam epitaxy are reported. The cadmium concentrations of the two materials are 0.18 for the bottom layer and 0.26 for the top. The measurements by Hall, *IV*, *CV*, and spectral responsivity are consistent with the existence of a conduction-band barrier at the interface behaving as an insulator at low temperature. We suggest that transient effusion cell fluxes occurring during shutter sequencing created such barriers at the heterojunction interfaces during the growth. The high R_0A (600 $\Omega \times cm^2$) measured suggests that this effect might be of interest for future heterojunction gate field-effect transistor investigations.

I. INTRODUCTION

The $Hg_{1-x}Cd_xTe$ (MCT) ternary alloy is currently the most important material for infrared applications in the 8–12 μm wavelength range. It is also used for the 3–5 μm window and considered for the optoelectronic range. This material can be grown for any cadmium composition x between 0 and 1, and can then be considered as a solid solution. The corresponding forbidden energy gap can be varied continuously between -0.22 and 1.6 eV at 80 K. These unique properties plus the fact that the lattice mismatch between the extreme compositions is only 0.3% make this ternary semiconductor material very attractive for heterojunction investigations. The main motivation for such studies is to improve existing detector performances by tailoring wavelength response, decreasing parasitic currents, and increasing minority-carrier collection efficiencies.

LoVecchio *et al.*[1] studied the case of back-to-back MCT ($x = 0.2$)/CdTe heterojunctions. They concluded that a valence-band barrier was present in the devices. *n/p* MCT heterojunction photovoltaic devices were demonstrated by Bratt.[2] In certain cases, barrier formation was also reported.

Both groups used the liquid phase epitaxy (LPE) growth technique and reported substantial grading and/or diffusion at the interfaces. Vydyanath *et al.*[3] showed that such effects could actually be profitable since they presented exceptional LPE grown MCT heterojunction detector performances.

The possibility of including semimetallic, semiconducting, and semi-insulating materials within the same monocrystal could lead to important technological applications. The abrupt heterojunctions between these materials have to be further studied.

Kuech and McCaldin[4] reported characterizations of HgTe layers grown by the metalorganic chemical vapor deposition technique at 325–350 °C on *n*-type CdTe. A Schottky barrier behavior was seen, with a maximum barrier height of 0.92 eV.

The validity of the common anion rule for the HgTe/CdTe system has been questioned recently.[5] The reported values of the valence-band offset vary from 40 meV (Ref. 6) to 350 meV[7,8] depending on the technique used. The above workers[4] mention that inversion in the CdTe layer could explain their low barrier height value. We suggest that interdiffusion effects might have played an important role. In any case, most of the band-gap difference should appear in the conduction-band discontinuity.

The molecular-beam epitaxy (MBE) technique is now recognized as a possible choice for the growth of MCT on CdTe and GaAs.[9,10] Its low growth temperature (190 °C) minimizes the interdiffusion effects and allows abrupt interfaces to be produced in thin epitaxial layers like superlattices. Several abrupt *n*-isotype heterojunctions between two narrow-band-gap compositions were grown for the first time in order to observe the transport properties of the electrons through the expected conduction-band discontinuity on the wide-band-gap side. We present here the characterization of mesa devices fabricated from these first samples.

II. EXPERIMENTAL

The junctions were grown on CdTe(111)//GaAs(100) substrates with a Riber 2300 system modified to handle mercury. Both sides of the junction were doped *n* type with indium as previously described.[11] The narrow-gap side was first made with a thickness of 2 to 3 μm before the growth conditions were abruptly changed to produce the wide-gap material up to a thickness of 1.0 μm. The substrate temperature was kept at 190 °C all along the growth. The composition of the narrow gap was determined by infrared transmission measurements at room temperature. Its doping level 4×10^{16} cm^{-3} was deduced from the Hall measurements neglecting the contribution of the wide-gap side. This was relevant since the doping level was intentionally lowered during the growth of the $x = 0.26$ material. The composition and doping ($\sim 5 \times 10^{15}$ cm^{-3}) of the top layer was estimated from the growth conditions on separate runs. To check the doping level, metal–insulator–semiconductor (MIS) structures were fabricated with gold and zinc sulfide on a different piece of the sample. The high-frequency capacitance versus voltage curves were measured at 80 K and 100 kHz with an LCR 4275 from Hewlett–Packard. The classical MIS calculation[12] was used to deduce the impurity level from the minimum to maximum capacitance ratio, where the minimum capacitance was calculated using the approximation of Ref.

 0734-2101/87/053119-05$01.00

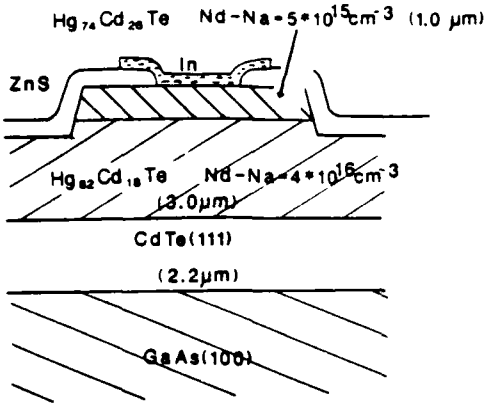

FIG. 1. Structure of the devices.

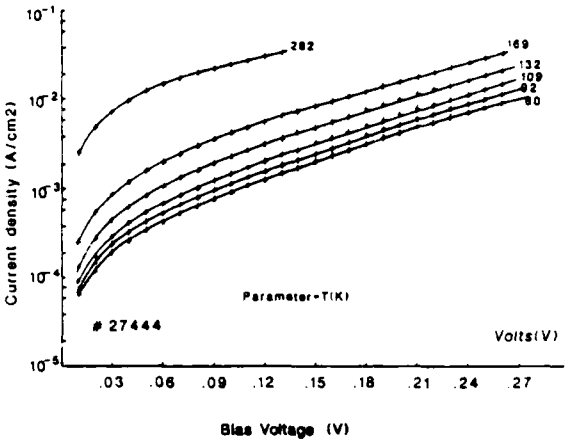

FIG. 3. Semilog plot of the I/V curves when the top material is biased negatively.

19. The doping level deduced was within a factor of 2 from the growth estimated value. The devices were made by standard photolithographic techniques and mesa etching. The metal was evaporated over the zinc sulfide passivation opened for contacts. Their structure can be seen in Fig. 1. The geometry is circular to minimize edge leakage but is obviously not optimized for detection applications. The junction area is 7×10^{-4} cm^2. More than 150 dots were tested from 300 down to 80 K with a microprobe station from MMR Technologies, Inc. The probe connected to the top contact was positioned on the metal part overlapping the zinc sulfide to avoid piezoelectric effects. The current versus voltage measurements were made with an electrometer/voltage source model 617 from Keithley, modified to generate 5-mV steps. All the data acquisition was computerized.

III. RESULTS

The current versus voltage curves measured can be seen in Fig. 2. They are representative of the average of the devices measured. Very weak forward rectification occurs when the top wide-band-gap material is biased negatively. They could be simply described as showing double soft reverse breakdown at low temperature. The current is proportional to the voltage at low bias, and tends to a power of the voltage law (2–3) above 50–100 mV. A semilogarithmic plot of these curves is shown in Fig. 3 for the forward bias case. Notice that their slopes are nearly independent of temperature. The R_0A values could reach 600 Ω cm^2 at 80 K on several devices, showing that the active part of the device is on the wide-band-gap side. Its variation as a function of $1/T$ can be seen in Fig. 4 in reverse bias. At high-temperature it follows an exponential law in a limited range only, and tends to saturate at low temperature. The corresponding high-temperature activation energies are systematically higher in reverse bias ($\sim$105 meV) than in forward bias ($\sim$80 meV). The I/V curves were fitted by the least-square method to the equation

$$I = I_s\{\exp[(V - IR_s)/V_0] - 1\}, \quad (1)$$

where I is the current density, I_s the saturated current den-

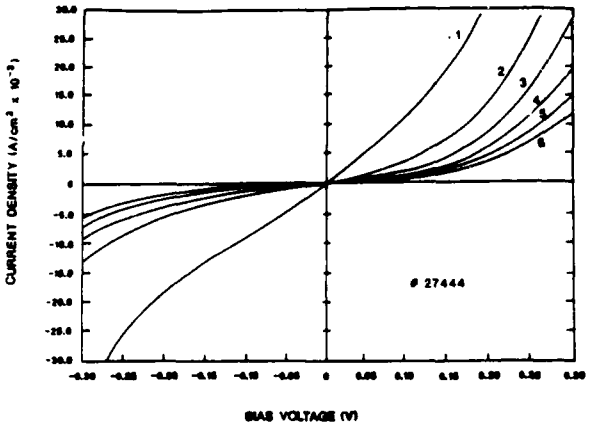

FIG. 2. Current/voltage curves vs temperature. Positive voltages correspond to negative bias on the top material. Temperatures: curve 1: 235 K, 2: 169 K, 3: 132 K, 4: 109 K, 5: 92 K, and 6: 80 K.

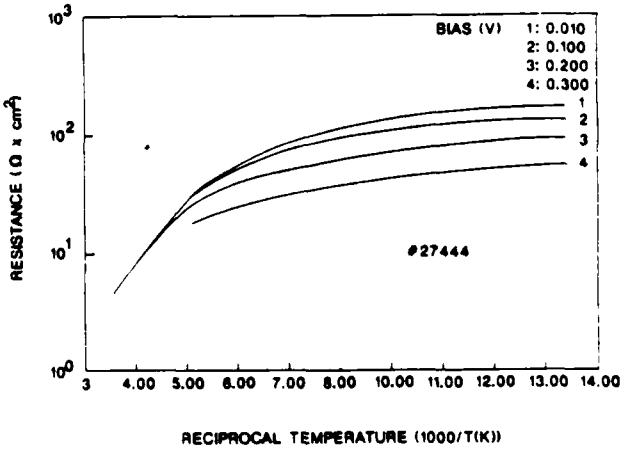

FIG. 4. Variation of the dc resistance of the device with reciprocal temperature.

sity, V the bias voltage, R_s the series resistance, and V_0 the voltage defining the slopes of the curves. The precision of the parameters extracted was only questionable close to room temperature where the devices showed an ohmic behavior. Below 150 K, V_0 was found constant and equal to 145 and 80 mV in reverse and forward bias, respectively, and R_s was negligible. V_0 was increasing with temperature above 150 K.

A typical capacitance versus voltage curve is shown in Fig. 5. It clearly does not follow the classical Schottky diode depletion model but rather a metal–insulator–semiconductor device behavior. The frequency dependence is small. The admittance curves correlate the slope variation of the dc current/voltage measurements.

IV. DISCUSSION

The lack of strong rectification implies that thermionic emission is negligible. The current transport is limited by some form of tunneling since it varies as $\exp(V/V_0)$ independently of temperature below 150 K. These properties are systematic for all the devices on several crystals, and are not resulting from a marginal contact process on the top contact which could create back-to-back Schottky diodes randomly. Furthermore, a sharp minimum in capacitance close to zero bias should be seen in this case.[13] Schottky barrier lowering with biasing voltage is not detected since the current should vary as $\exp(\alpha V^{1/4}/T)$,[12] and V_0 should be a function of temperature even at 80 K.

These results have similarities with the theory of thermionic field emission across Schottky barriers (TFS).[14] The ratio kT/E_{00} is an estimation of the relative importance of the thermionic and field emission processes,[15] where k is the Boltzmann constant, T the absolute temperature, and E_{00} an energy defined as

$$E_{00} = (qh/4\Pi)(N_D/m^*\epsilon)^{1/2}, \tag{2}$$

where q is the electronic charge, h the Planck's constant, N_D the donor concentration in the semiconductor (in our case the wide-band-gap side with $x = 0.26$), m^* and ϵ the electron effective mass and the static dielectric constant in the same material. When $kT \gg E_{00}$ the current is mainly due to thermionic emission. When $kT \ll E_{00}$ field emission (or tunneling from energies close to the conduction band) is the dominant transport mechanism. Both types of electron emission have to be considered when $kT \simeq E_{00}$. In our case $N_D \simeq 5\times10^{15}$ cm^{-3}, and for $x = 0.26$ at $T = 80$ K, the relative electron effective mass and dielectric constant are taken, respectively, as 1.4×10^{-2} and 16.9. The value of E_{00} is then 2.66 meV, much smaller than $kT = 6.9$ meV. The fact that thermionic conduction is not seen in forward bias, together with the capacitance measurements results, make us conclude that a large conduction-band barrier is present at the heterojunction between the two materials. This is in agreement with the spectral response measured on one device in small reverse bias at 80 K, showing a wide response in the 3–6 μm range and a peak more than three times higher in amplitude at 1.9-μm wavelength. The root square of the photoresponse is shown versus wavelength in Fig. 6. The low-energy tail was close to the noise floor and was separated from the response of the $x = 0.26$ material by more than 1 μm. The measurement was made under vacuum with a glow bar infrared source, a monochromator, and a lock-in amplifier. The curve was corrected for blackbody radiation and grating dispersion. It can be interpreted as internal photoemission from a conduction-band barrier 0.56 eV above the Fermi level (being degenerate in the narrow-band-gap material). The TFS theory predicts that the current/voltage relation should be of the form[14]

$$I = I_s \exp(qV/E_0)$$

at high enough voltages, where $E_0 = E_{00}\coth(E_{00}/kT)$ and I_s is a function of T, the barrier height, the doping level, and is a weak function of the bias. E_{00} has been previously introduced.

Since $E_0 = 80$ meV below 150 K in our devices, we can see that the rise in E_0 above this temperature cannot be accounted for by the TFS theory. Tunneling through a high and

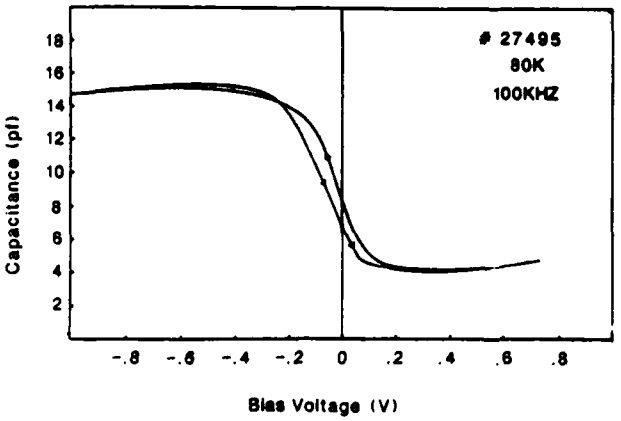

FIG. 5. High-frequency capacitance/voltage curve at low temperature. Positive voltages correspond to positive bias on the top material.

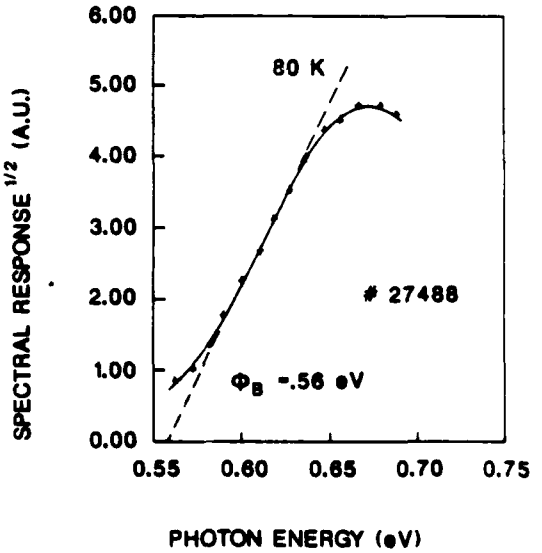

FIG. 6. Root square of the spectral response of the device vs photon energy. Only the high-energy tail is shown.

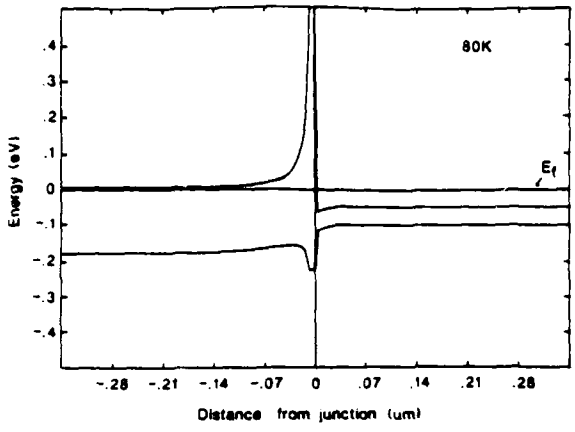

FIG. 7. Calculation of the assumed band profile of the structure at zero bias. Parameters used: $m^*_{HH}/m_0 = 0.44$, doping left-hand side $= 5\times10^{15}$ cm^{-3}, doping right-hand side $= 4\times10^{16}$ cm^{-3}, Cd composition left-hand side $= 0.26$, Cd composition right-hand side $= 0.18$, Cd composition at the barrier peak $= 0.6$, $\Delta E_v = 0.15\times\Delta E_g$. $T = 80$ K.

sharp barrier is the suspected dominant transport at low T. Only a minor contribution to the current is due to band bending change with bias in the $x = 0.26$ material. As will be discussed later, we think that the barrier resulted from abrupt composition change during growth. Its actual conduction-band profile is expected to be much steeper than the parabolic potential approximation made in the TFS theory.

A Poisson solution of the expected band profile of the device at 80 K is shown in Fig. 7. An abrupt Cd composition increase up to $x = 0.6$ was assumed right at the interface, followed by a sharp exponential decrease down to $x = 0.26$. The minimum barrier thickness was set to be 100 Å. The valence-band offset between two different composition materials was assumed to be 15% of their band-gap difference. A heavy-hole effective mass independent of composition and equal to 0.44 has been used. The calculation is made with the relaxation method, using the two-band Kane[16] model and assuming fully ionized dopants without diffusion effects at the interface. Degeneracy is included. The details of this calculation will be presented elsewhere.[17] We can see that the Fermi level on the left-hand side is within 1 meV of the conduction band, whereas the narrow bandgap is heavily degenerate, the Fermi level lying 45 meV above the conduction band.

This structure basically looks like a metal–insulator–semiconductor device as suspected from the capacitance measurements. The semiconductor with $x = 0.26$ is weakly degenerate. The use of a metal–insulator–metal tunneling model could be appropriate at low temperature where we established that tunneling transport is dominant. We used the model developed by Simmons[18] for its simplicity, modifying it slightly to make provision for different effective masses in the metal and the insulator. It assumes a rectangular barrier and is restricted to low temperatures where the tunneling is independent of temperature. We did not use it in the first place since it cannot demonstrate the existence of the tunneling process by itself. The current density is given by

$$I = (1/R_0)\{(\Phi_B - V/2)\exp(-A\sqrt{\Phi_B - V/2}) - (\Phi_B + V/2)\exp(-A\sqrt{\Phi_B + V/2})\}$$

with $A = 4\Pi d\sqrt{2m_i q}/h$,

$$R_0 = (2\Pi h d^2/q^2)(m_i/m_m),$$

$V < \Phi_B$, d is the thickness of the barrier, Φ_B the barrier height, V the bias, h the Planck's constant, and q the electronic charge. m_i^* and m_m are the electron effective masses in the insulator and the metal electrode acting as the cathode, respectively. R_0 is not to be confused with the zero bias resistance of the device.

The effect of barrier height lowering is not considered since it could not be detected from the measurements and the barrier height is expected to be large. The fact that the curves in Fig. 3 are nearly symmetric is consistent with this model. The low-temperature curve of Fig. 3 was fitted in reverse bias since the tunneling is less affected then in forward bias by the actual barrier profile on the wide-band-gap side. Φ_B and d where adjusted to produce the results shown in Fig. 8. The following effective masses have been used: $m_i/m_0 = 0.058$ and $m_m^*/m_0 = 0.0039$. It can be seen that the best fit occurs for $\Phi_B \simeq 0.55$ eV, in excellent agreement with the optical result. The average matching barrier thickness is close to 110 Å.

The capacitance measurements can be interpreted as follows: the diode is essentially behaving as an MIS where the narrow-band-gap material is the metal electrode and the barrier is the insulator. The top semiconductor with $x = 0.26$ is then seen n-type in depletion at zero bias. Calculation of the low-frequency differential capacitance of the structure shown in Fig. 7 was attempted using the same type of calcu-

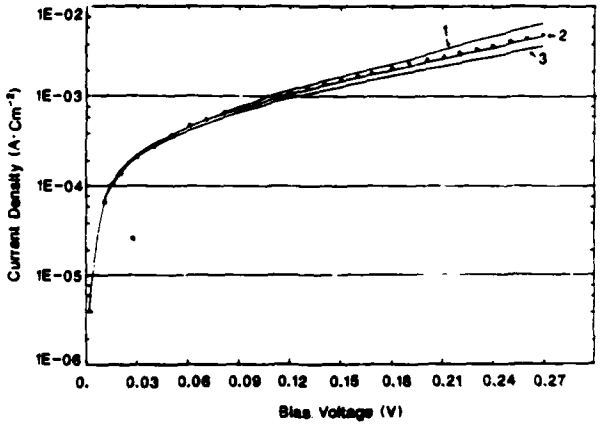

FIG. 8. Fitting of the Simmons model to the low-temperature curve of Fig. 2. The top material is biased positively. Parameters used:

	Φ_B (eV)	d (Å)
Curve 1	0.45	119
Curve 2	0.55	109
Curve 3	0.65	101

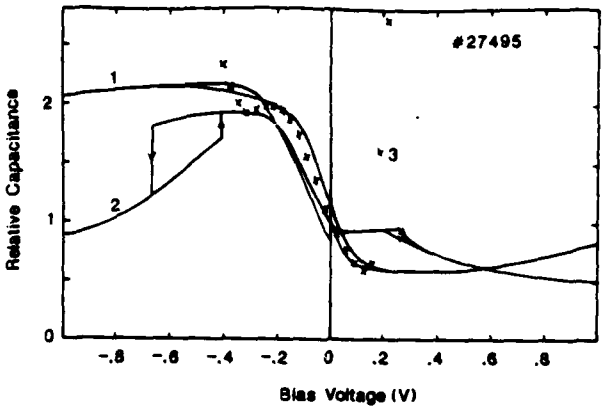

FIG. 9. Relative capacitance vs voltage curves. Curve 1: second measurement of the *CV* data shown in Fig. 5. $T = 80$ K, 100 kHz. Curve 2: measurement of the same device with the same frequency. $T = 160$ K. Curve 3 = × Low-frequency capacitance calculation at 80 K. Same parameters as in Fig. 7.

lation as before and the same parameters. The quasi-Fermi levels on each side of the heterojunction were assumed to be constant, their difference being abruptly accommodated at the interface. The result is shown in Fig. 9, together with measurements made at 80 and 160 K at 100 kHz on the same device. We can see that an accumulation plateau occurs below -0.2 V. Its magnitude is much smaller than the capacitance of the pseudoinsulator alone. This is due to the onset of depletion on the narrow-band-gap side which begins to be inverted below -0.3 V. The high-frequency low-temperature *CV* curve then stays approximately constant thereon. The calculation also shows strong inversion of the wide-band-gap side to be occurring at $+0.15$ V. Notice that these thresholds tend to precede the abrupt falls in capacitance measured at 160 K. We think that these transitions are linked to the collapse of their corresponding hole inversion layers through the valence side of the burst barrier, driving their respective material side in deep depletion. It demonstrates that hole confinement against this barrier occurred before. We conclude that a valence-band barrier is also present, and that the valence-band offset cannot be neglected. Even though no precise value can be deduced from this work, we should point out that the 15% of the band-gap difference value used in the calculations is consistent with all the measurements made as well as the recently published studies[7,8] when extrapolated to the HgTe/CdTe case. At the present time the reason why the capacitance only collapses at high temperatures is not clearly understood. It might be linked to two-dimensional quantized energy levels of the inversion layers interacting with deep levels within the bursting material. Even though the deep levels have been omitted from this study, they are known to be present since noticeable hysteresis has been seen in the *CV* measurements, and to a smaller degree in the *IV* measurements. They could also contribute to the enhanced tunneling process described.

The burst in composition which occurred at the interface is linked to the transient flux response of the effusion cell opened during the growth to increase the cadmium content of the top layer. When the shutter is closed, the cell has a higher quasiequilibrium pressure than with the shutter opened. This study shows that with the particular geometry used the time constant required by the cell to change from the closed to opened stable conditions was in the order 8 s. Once detected, this problem can be avoided. Recently grown devices trying to avoid this effect give credit to this hypothesis and will be published later.

V. CONCLUSION

We showed that the electrical characterizations of the first abrupt *n*-isotype heterojunctions made by MBE were consistent with the presence of a sharp burst in composition at the heterojunction interface due to the growth conditions.

The measurements and the calculations presented are in agreement with the presence of a valence-band offset between the barrier material and the adjacent layers. When extrapolated linearly to the HgTe/CdTe case, the value assumed is in agreement with the recently published studies. The high R_0A values obtained even for a narrow-gap composition $x = 0.17$ could be of interest for future gate field-effect transistor investigation.

ACKNOWLEDGMENTS

This work was funded by DARPA Contract No. MDA903-85K-0030. One of us (M. E. D.) has also a scholarship from CNPq-Brazil.

[1] P. LoVecchio, M. B. Reine, and M. N. Grimbergen, J. Vac. Sci. Technol. A 3, 246 (1985).
[2] P. R. Bratt, J. Vac. Sci. Technol. A 1, 1687 (1983).
[3] H. R. Vydyanath, S. R. Hampton, P. B. Ward, L. Fishman, J. Slawinski, and T. Krueger, 1986 IRS Detector Specialty Group Meeting, NASA AMES Research Center, Moffet Field, CA.
[4] T. F. Kuech and J. O. McCaldin, J. Appl. Phys. 53, 3121 (1982).
[5] J. Tersoff, Phys. Rev. Lett. 56, 2755 (1986).
[6] Y. Guldner, G. Bastard, J. P. Vieren, M. Voos, J. P. Faurie, and A. Million, Phys. Rev. Lett. 51, 907 (1983).
[7] S. P. Kowalczyk, J. T. Cheung, E. A. Kraut, and R. W. Grant, Phys. Rev. Lett. 56, 1605 (1986).
[8] T. M. Duc, C. Hsu, and J. P. Faurie, Phys. Rev. Lett. 58, 1127 (1987).
[9] J. P. Faurie, A. Million, R. Boch, and J. L. Tissot, J. Vac. Sci. Technol. A 1, 1593 (1983).
[10] J. P. Faurie, S. Sivananthan, M. Boukerche, and J. Reno, Appl. Phys. Lett. 48, 1307 (1984).
[11] M. Boukerche, J. Reno, I. K. Sou, C. Hsu, and J. P. Faurie, Appl. Phys. Lett. 48, 1733 (1986).
[12] S. M. Sze, *Physics of Semiconductor Devices*, 2nd ed. (Wiley, New York, 1981).
[13] C. N Van Opdorp, thesis, Technical University of Eindhoven, 1969.
[14] F. A. Padovani and R. Stratton, Solid State Electron. 9, 695 (1966).
[15] C. R. Crowell and V. L. Rideout, Solid State Electron. 12, 89 (1969).
[16] E. O. Kane, J. Phys. Chem. Solids 1, 249 (1957).
[17] M. Boukerche and J. P. Faurie, Solid State Electron. (submitted).
[18] J. G. Simmons, J. Appl. Phys. 34, 1793 (1963).
[19] E. H. Nicollian and J. R. Brews, *MOS (Metal Oxide Semiconductor) Physics and Technology* (Wiley, New York, 1982), p. 164.

Hg incorporation in CdTe during the growth of HgTe-CdTe superlattices by molecular beam epitaxy

J. Reno,[a] R. Sporken,[b] Y. J. Kim, C. Hsu, and J. P. Faurie
Department of Physics, University of Illinois at Chicago, Chicago, Illinois 60680

(Received 3 August 1987; accepted for publication 9 September 1987)

HgTe-CdTe superlattices and other microstructures such as single and double barrier tunneling structures are commonly grown by molecular beam epitaxy with the mercury flux continuously on the sample during the growth. This means that some mercury will be incorporated in the CdTe layers. We present here, for the first time, a measurement of the amount of mercury incorporated in thin layers of CdTe. X-ray photoelectron spectroscopy was used to measure the amount of mercury. The amount of mercury was found to be between 3 and 9% for CdTe (111)*B*, depending on the growth conditions. The amount of mercury was found to increase with mercury flux and to decrease as the substrate temperature was increased. Under the same conditions, it was found that much more mercury was incorporated in the (100) orientation. The type of substrate (CdTe or GaAs) was not found to influence the results. These results indicate that the amount of mercury in the CdTe layers of HgTe-CdTe superlattices is not quite as low as expected from measurements of thick CdTe layers, but it can be low enough that it does not influence significantly the results on the superlattice system in the (111) orientation.

HgTe-CdTe superlattices have been proposed as a new, interesting infrared material.[1,2] It has been shown that they can be grown by molecular beam epitaxy (MBE).[3] It has also been shown that the best growth temperature is 180–200 °C.[3] At this temperature the mercury condensation coefficient is about 10^{-3}.[4] This means that a large mercury overpressure is needed to grow HgTe. It also implies that mercury will easily and noncongruently evaporate from HgTe. Due to this problem, the common growth technique for HgTe-CdTe superlattices and other microstructures such as single and double barrier tunneling structures involves leaving the Hg source open at all times.[5,6] Thus, there is a mercury flux on the sample during the growth of the CdTe layers. A competition then occurs between the Hg and Cd atoms for lattice sites. As a result, the CdTe layers may not be pure CdTe but instead be $Hg_{1-x}Cd_xTe$ with some percentage of mercury.

This problem was recognized by the first people to grow HgTe-CdTe superlattices on CdTe (111)*B* substrates. They grew thick layers of CdTe under the same conditions as in the superlattice, including the presence of the Hg flux. The Hg content was then measured by energy dispersive spectroscopy (EDS). It was found that the CdTe contained less than 5% mercury.[7] When we began to grow HgTe-CdTe superlattices at the University of Illinois, we repeated these experiments with the same results.[5] This small amount of mercury should only slightly influence the characteristics of the superlattices such as the band gap and the valence-band discontinuity. Therefore, it was neglected. The only question was whether the results for a thick layer were the same for the thin layer in the superlattice.

Recently, it has been suggested that the amount of mercury in the CdTe layers of the superlattice might not be as small as previously thought.[8] For this reason we have performed the first measurements of the amount of mercury incorporated in *thin* CdTe layers grown with a mercury flux. We have also looked at how the amount of mercury incorporated depends upon the substrate temperature, the mercury flux, the CdTe growth rate, and on the type and orientation of the substrate.

The samples were all grown at the University of Illinois in a Riber 2300 MBE machine. CdTe substrates oriented in the (100) and the (111)*B* were used. Additionally, GaAs(100) with both (100) and (111)*B* CdTe buffer layers were used. The substrate preparation and the growth of the appropriate buffer layer have been discussed elsewhere.[5] The Te flux was kept constant throughout the experiment. The flux was chosen so that the HgTe growth rate was about 5 Å/s on a CdTe(111)*B* substrate. A CdTe growth rate of 1 Å/s was used throughout the experiment, except when that growth rate was the parameter being varied. These growth rates are typical of those used in the growth of HgTe-CdTe superlattices. The substrate temperature was measured using a chromel-alumel thermocouple in contact with the sample holder and by an infrared pyrometer. These measurements have been calibrated using the melting temperatures of indium and tin.

The structure of the samples was chosen to be similar to that of the superlattices. On the buffer layer a HgTe layer with a thickness of 80–100 Å was grown first. This was immediately followed by a CdTe layer 150–170 Å thick. The CdTe layer was grown with the Hg flux still on the sample. The Hg concentration in the CdTe layers was measured by x-ray photoelectron spectroscopy (XPS) using both the ratio of peak areas and the energy difference between the Hg 5*d* or Cd 4*d* core level and the valence-band maximum (VBM). For $Hg_{1-x}Cd_xTe$, this energy difference can be shown to reflect the position of the VBM on an absolute energy scale, because the cation core levels are virtually independent on the alloy composition x.[9,10] The position of the VBM is

[a] Present address: Sandia National Laboratory, Organization 1144, Albuquerque, NM 87185.
[b] Permanent address: Facultes Universitaires Notre-Dame de la Paix, B-5000 Namur, Belgium.

 0003-6951/87/451545-03$01.00

known in turn to be very sensitive to the composition x.[9,10] Therefore, the binding energy of the Hg 5*d* and Cd 4*d* core levels with respect to the VBM can be used to determine the alloy composition x. Several samples were grown without the HgTe layer on the bottom to see if its presence changed the measurement. No difference was found in the Hg concentration in the CdTe whether the HgTe was present or not. First with the Te and CdTe fluxes constant, the substrate temperature and the Hg flux were varied to determine their influence on the Hg incorporation.

The samples were kept under ultrahigh vacuum conditions as they were transferred to the XPS chamber. The XPS measurements were performed with an SSX-100 spectrometer from Surface Science Laboratories. A monochromatized and focused Al $K\alpha$ excitation line was used. The overall energy resolution measured on the Au $4f_{7/2}$ core level is 0.7 eV. The core levels used in this work were the Hg 4*f* and 5*d*, the Cd 4*d* and 3*d*, and the Te 4*d* and 3*d*. The values of the peak areas and positions of all the core levels were determined by a detailed analysis of the spectra by a least-squares fit of individual spin-orbit doublets to the data. The line shape used for the fits was a Lorentzian convoluted with a Gaussian. A nonlinear background was subtracted from the spectra prior to the fitting procedure.

Figure 1 shows a typical result for the spectrum of the Cd 4*d* and the Hg 5*d* core levels. This is the most difficult case due to the large number of overlapping peaks. The fit reveals the existence of two Hg components. These two components will be called $Hg^{(1)}$ and $Hg^{(2)}$ in the following discussion. From its binding energy with respect to the VBM,[10] $Hg^{(1)}$ can be clearly identified as Hg in $Hg_{1-x}Cd_xTe$. The origin of $Hg^{(2)}$, at about 600 meV higher binding energy, is not yet fully understood. We believe that $Hg^{(2)}$ is some sort of surface mercury. Further experiments are still in progress to clarify this point. Only the component $Hg^{(1)}$, associated with Hg in $Hg_{1-x}Cd_xTe$, was used in our measurements. It

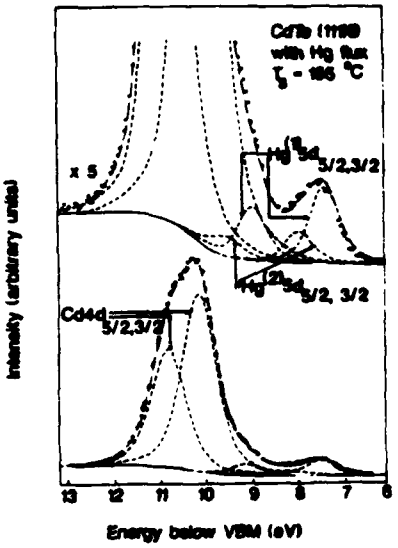

FIG. 1. Typical XPS spectrum from a CdTe layer grown with a mercury flux. The dash-dotted line is the result of a least-squares fit to the data. The dashed lines represent the individual components used for this fit. The background is represented by the solid line. The dots are the experimental data.

is the only one that should influence the band gap, if $Hg^{(2)}$ is indeed a surface phenomenon.

To obtain the binding energies ($E_{Cl} - E_V$) used for the determination of the Hg concentration, the position of the VBM was determined simply by a linear extrapolation of the valence-band leading edge. This procedure has proven to be reproducible and very accurate for Te-based II-VI semiconductors.[11] Since the binding energy defined above is very sensitive to the Hg concentration in $Hg_{1-x}Cd_xTe$,[10] it can be used to determine the amount of Hg in the CdTe. As can be seen in Table I, there is good agreement between the two methods. This gives us confidence in our results and in neglecting the $Hg^{(2)}$ component. This procedure implies the measurement of the valence-band energy distribution curve and is thus highly time consuming. Therefore, it was not applied systematically to all the samples.

In order to compare our previous results for a thick layer with these for a thin layer, we grew a thick CdTe layer and checked the Hg concentration with both XPS and EDS. The growth conditions were similar to those used for the thin layers (T_s = 195 °C, Hg flux = 1.6×10^{17} cm^{-2} s^{-1}, and CdTe growth rate 1 Å s^{-1}). The results from EDS agreed with all of our earlier work and gave a value of about 3% Hg in the CdTe. The XPS results on this layer gave a Hg concentration of 5%. This difference is within the range of experimental error, but it may also indicate that there is a slight difference in the Hg concentration with depth.

The homogeneity of the Hg distribution with depth can be checked by comparing results from core levels at different binding energies. In our case the determinations using the Hg 4*f*, Cd 3*d*, and Te 3*d* core levels are more surface sensitive than those using the Hg 5*d*, Cd 4*d*, and Te 4*d* lines. This is due to the smaller escape depth for the Cd 3*d* and Te 3*d* photoelectrons ($\lambda \simeq 15$ Å) compared to the Cd 4*d* and Te 4*d* ($\lambda \simeq 20$ Å). We found that the more surface-sensitive determinations systematically yielded slightly higher concentrations. Compared with EDS, XPS is primarily a surface technique. The observed surface enrichment is thus consistent with the difference between the bulk results from EDS and the XPS results. Further investigations with good depth resolution would certainly be very desirable to confirm (or infirm) this point.

Table I summarizes the Hg concentrations determined by XPS for the different substrate and Hg cell temperatures. The Hg concentrations determined by both XPS methods are given. The values given in the table based on peak area

TABLE I. Hg to Te ratio in CdTe grown with a Hg flux on CdTe substrates, along with the growth conditions. T_s is the substrate temperature. The CdTe growth rate was held constant at about 1 Å/s.

Substrate orientation	T_s (°C)	Hg flux (10^{17} cm^{-2} s^{-1})	$1-x$ (area ratios)	$1-x$ (binding energies)
(111)*B*	175	1.6	0.085 ± 0.009	0.087 ± 0.020
(111)*B*	185	1.6	0.065 ± 0.015	0.051 ± 0.020
(111)*B*	195	1.6	0.057 ± 0.016	...
(111)*B*	195	0.89	0.045 ± 0.010	0.070 ± 0.020
(111)*B*	195	1.6	0.057 ± 0.016	...
(111)*B*	195	2.2	0.085 ± 0.016	0.100 ± 0.020
(100)	185	1.6	0.147 ± 0.016	...

ratios are average values from four different sets of core level spectra. Relative sensitivity factors were determined for our instrument from MBE grown HgTe (111) and CdTe (111) samples.

The Hg flux was determined using Knudsen's effusion law, which is a good approximation in this case for the direction normal to the evaporating surface. A change of the substrate temperature by 10 °C will change the Hg condensation coefficient by about a factor of 1.5.[4] Several striking features are observed from this table. First, for these growth conditions on CdTe (111)*B* the amount of Hg incorporated is much less than 20%.[12] Second, the overall agreement between the area ratio and the binding energy results is good. Third, the amount of Hg incorporated follows the general trends expected from the growth conditions, and the relative magnitudes are in reasonable agreement with the Hg flux and condensation coefficient variations. Fourth, a Hg concentration of 5% was obtained by the correct selection of the growth conditions and we have obtained a value as low as 3% in a second set of experiments.

It has been reported that for a CdTe (211) substrate the amount of Hg incorporated is about 20%.[13] We have also shown that the Hg condensation coefficient varies depending on the orientation of the substrate.[14] For this reason, we have also investigated CdTe (100). The fluxes were the same as used for the (111)*B*. The results are also given in Table I. The difference in the Hg incorporation is very large and opposite to our initial expectations, since Hg on CdTe (100) has the smaller condensation coefficient of these two orientations. We do not understand these results, but they show once again that MBE growth cannot be treated by a classical thermodynamic approach using the law of mass action and neglecting surface kinetics.

We performed a second set of experiments to check the dependence of the Hg incorporation on the CdTe growth rate and on the type of substrate. The Te and Hg fluxes were kept constant. The results are given in Table II.

The first point that can be seen from these results is that it does not matter whether a CdTe (111)*B* substrate or a GaAs (100) substrate with a CdTe (111)*B* buffer is used to grow the layers. The Hg incorporation is about the same for the two different substrates. The second point is that the Hg incorporation appears to increase with the CdTe growth rate. We do not have much data, but the trend appears to be in this direction.

It was also found that the quality of the surface prior to the growth of our structures could dramatically influence the amount of Hg incorporated. If the same substrate was reused frequently and thus re-etched several times or an inadequate buffer layer was grown, a significantly larger Hg incorporation was found. This means that extreme care must be taken not only when doing this type of experiment but also when preparing a substrate on which to grow a superlattice.

In conclusion, we have presented for the first time a measurement of the amount of mercury incorporated in thin layers of CdTe grown under mercury flux. The growth conditions and the structures were chosen to be similar to those in HgTe-CdTe superlattices. When carefully prepared, layers grown on CdTe (111)*B* were found to contain between 3 and 9% mercury. The amount of mercury was found to increase with the mercury flux and the CdTe growth rate, and to decrease as the substrate temperature was increased. We did not observe any significant dependence of the amount of mercury incorporated on the type of substrate but there was a large dependence on the orientation of the substrate. We found that much more mercury was incorporated for (100) than for (111)*B* prepared under the same conditions. We thus expect the Hg incorporation in CdTe (100) to be even more important under normal growth conditions.[14] This dependence of the amount of mercury incorporated on the growth conditions and the substrate orientation means that care must be taken when comparing results between different groups. Also, dramatic increases in the amount of Hg incorporated can occur if the initial surface is not properly prepared. These results indicate that the amount of mercury incorporated into carefully prepared (111)*B* superlattices is small enough that it should not significantly influence the characteristics of the superlattices previously reported, and in particular the value of the valence-band discontinuity and the band gaps.

TABLE II. Hg to Te ratio in CdTe grown with a Hg flux along with the growth conditions. All were grown on a CdTe (111)*B* buffer layer but the initial substrate was varied. T_s is the substrate temperature. Estimated Hg flux: 1.6×10^{17} cm^{-2} s^{-1}.

Substrate	T_s (°C)	CdTe growth rate (Å/s)	$1-x$ (area ratios)	$1-x$ (binding energies)
CdTe	195	0.5	0.030 ± 0.004	0.043 ± 0.020
CdTe	195	1.0	0.057 ± 0.016	...
CdTe	195	2.0	0.078 ± 0.008	...
GaAs	185	1.0	0.065 ± 0.007	0.043 ± 0.020
GaAs	195	1.0	0.036 ± 0.008	...

This work carried out at the University of Illinois at Chicago was supported by the Defense Advanced Research Projects Agency and monitored by the Air Force Office of Scientific Research under contract No. F4920-87-C-0021. One of us (R. S.) is supported in part by the National Belgian Foundation for Scientific Research (FNRS).

[1] J. N. Schulman and T. C. McGill, Appl. Phys. Lett. 34, 663 (1979).
[2] D. L. Smith, T. C. McGill, and J. N. Schulman, Appl. Phys. Lett. 43, 180 (1983).
[3] J. P. Faurie, A. Million, and J. Piaguet, Appl. Phys. Lett. 41, 713 (1982).
[4] J. P. Faurie, A. Million, R. Boch, and J. L. Tissot, J. Vac. Sci. Technol. A 1, 1593 (1983).
[5] J. P. Faurie, IEEE J. Quantum Electron. QE-22, 1656 (1986).
[6] K. A. Harris, S. Hwang, D. K. Blanks, J. W. Cook, J. F. Schetzina, N. Otsuka, J. P. Baukus, and A. T. Hunter, Appl. Phys. Lett. 48, 396 (1986).
[7] J. P. Faurie, A. Million, and J. Piaguet (unpublished results, 1982).
[8] S. Parkowitz, D. Rajavel, I. K. Sou, J. Reno, J. P. Faurie, C. E. Jones, T. Casselman, K. A. Harris, J. W. Cook, and J. F. Schetzina, Appl. Phys. Lett. 49, 806 (1986).
[9] C. K. Shih and W. E. Spicer, Phys. Rev. Lett. 58, 2594 (1987).
[10] C. Hsu, T. M. Duc, and J. P. Faurie (unpublished).
[11] T. M. Duc, C. Hsu, and J. P. Faurie, Phys. Rev. Lett. 58, 1127 (1987).
[12] S. Parkowitz, R. Sudharsanan, and S. S. Yom, J. Vac. Sci. Technol. A 5, 3157 (1987).
[13] M. W. Goodwin, M. A. Kinch, R. J. Koestner, M. C. Chen, D. G. Seiler, and R. J. Justice, J. Vac. Sci. Technol. A 5, 3140 (1987).
[14] S. Sivananthan, X. Chu, J. Reno, and J. P. Faurie, J. Appl. Phys. 60, 1359 (1986).

To appear in Physics and
applications of quantum
wells and superlattices
edited by K. von Klitzing
and E.E. Mendez
Plenum - New York

Molecular Beam Epitaxial Growth and Properties of Hg-based Microstructures

Jean-Pierre Faurie

Department of Physics
University of Illinois at Chicago
P.O. Box 4348, Chicago, IL 60680

ABSTRACT

This review paper reports on growth by Molecular Beam Epitaxy and characterization of $Hg_{1-x}N_xTe$-CdTe (N = Cd, Mn or Zn) superlattices and $Hg_{1-x}Cd_xTe$-HgTe heterojunctions with a special attention to the interdiffusion, the valence band offset between HgTe and CdTe and the Type III to Type I transition in these superlattices.

I. INTRODUCTION

HgTe-CdTe superlattices have received a great deal of attention over the last several years as a potential material for far-infrared detectors. Since 1979 when this superlattice (SL) system was first proposed as a new material for application in infrared optoelectronic devices,[1] significant theoretical and experimental attention has been given to the study of this new superlattice system. The interest in HgTe-CdTe SL is due to the fact that it is a new structure involving a II-VI semiconductor and a II-VI semimetal and that it appears to have great potential as a material for infrared detectors.

Most of the studies have focused primarily on the determination of the superlattice bandgap as a function of layer thicknesses and as a function of temperature. Also, the description of the electronic and optical properties at energies close to the fundamental gap has received much attention.[2-4]

The growth of this novel superlattice was first reported in 1982[5] and has subsequently been reported by several other groups.[6-9]

The first theoretical calculations using either the tight binding approximation with spin orbit splitting[1] or the envelope function approximation[2]

showed that the bandgap E_g of the SL did vary from 0 to 1.6V demonstrating that it could possibly used as an infrared material. These first calculations assumed that the valence band offset $A = \Gamma_{8HgTe} - \Gamma_{8CdTe}$ was small or even zero in agreement with the phenomenological common anion rule.[10]

Theoretical calculations predict a narrowing of the SL bandgap E_g compared to the bandgap of the $Hg_{1-x}Cd_xTe$ alloy with the same composition. Also the SL bandgap is predicted to decrease as the thickness of the HgTe layer (d_1) in the superlattice increases. It has also been predicted that in the far infrared the cutoff wavelength of the SL will be easier to control than that of the corresponding alloy since $d\lambda/d(d_1)$ of the SL should be less than $d\lambda/dx$ of the alloy.[3] These three predictions have been confirmed experimentally.[11-14] In the classification proposed for heterointerfaces,[15] the HgTe-CdTe SL appears to belong to a new class of superlattices called Type III. This is due to the inverted band structure (Γ_6 and Γ_8) in the zero gap semiconductor HgTe as compared to those of CdTe, which is a normal semiconductor [Fig. 1]. Thus, the Γ_8 light-hole band in CdTe

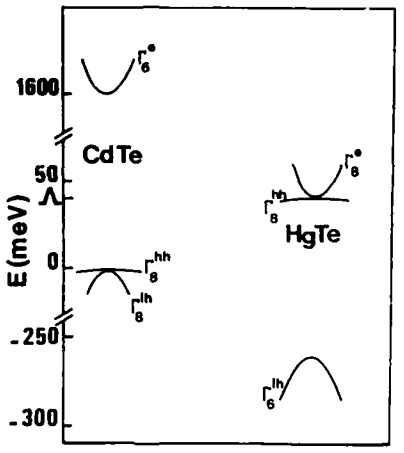

Fig. 1. Band structure of bulk HgTe and CdTe. The lh, hh and e indices refer to light holes, heavy holes and electron respectively.

becomes the conduction band in HgTe. When bulk states made of atomic orbitals of the same symmetry but with effective masses of opposite signs are used, the matching up of bulk states belonging to these bands has, as a consequence, the existence of a quasi-interface state which could contribute significantly to optical and transport properties.[16] Indeed, we have shown that the interface states could be responsible for the high hole mobilities prviously reported and not yet understood.[17,18]

investigations, the orientation of the CdTe film is the $(\overline{III})$Te face.[22] We have grown on both CdTe$(\overline{III})$//GaAs(100) and CdTe(100//GaAs(100) substrates and we have seen a difference in the mercury condensation coefficient. This has already been reported for the growth of $Hg_{1-x}Cd_xTe$ films on substrates of different crystallographic orientations.[23] It turns out that growing at 190°C on a (100) orientation requires about 4.4 times more mercury than growing on a $(\overline{III})$Te orientation at the same temperature. But in the (100) orientation no microtwinning due to the formation of antiphase boundaries are observed which makes the growth more easy to control than in the $(\overline{III})$B orientation.

In order to obtain high quality superlattices we use typical growth rates of 3-$Å s^{-1}$ for HgTe and $1Å s^{-1}$ for CdTe. This represents the best compromise between the low growth rate required for high crystal quality, especially for CdTe which should be grown at a higher temperature than 180°C, and the duration of the growth, which should be as short as possible in order to save mercury and to limit the interdiffusion process which cannot be completely neglected between these interfaces (this will be discussed later).

Compared to the growth of HgTe-CdTe SL that of $Hg_{1-x}Cd_xTe$-CdTe SL presents an additional difficulty since we have to control the ternary alloy $Hg_{1-x}Cd_xTe$ instead of the binary compound HgTe. Furthermore, since our goal is the study of the Type III - Type I transition, the composition (x) of the alloy should be very well controlled. In order to have the necessary flexibility for the composition x, a Cd cell plus a CdTe cell or two CdTe cells are required. The growth of $Hg_{1-x}Cd_xTe$ by MBE has already been discussed in numerous papers[24] and the growth of $Hg_{1-x}Cd_xTe$/CdTe SLs successfully achieved.[18]

$Hg_{1-x}Mn_xTe$-CdTe SLs have been grown with x ranging from 0.02 to 0.12 on CdTe$(\overline{III})$//GaAs(100) substrates using three effusion cells containing Hg, Mn and Te for the growth of the alloy and a CdTe cell for the growth of CdTe.[25]

More recently $Hg_{1-x}Zn_xTe$-CdTe SLs have been grown with x ranging from 0.02 to 0.15 on CdTe$(\overline{III})$//GaAs(100) substrates using three effusion cells containing Hg, Te and ZnTe for the growth of the alloy and a CdTe cell for the growth of CdTe.

The proof that these novel superlattice systems have successfully been grown is attested to by X-ray diffraction, as illustrated in Fig. 2. In addition to the Bragg peak one can see satellite peaks due to the new periodicity. The periods of the SLs were measured from the position of the SL satellite peaks as determined by X-ray. The method for determining the period of a superlattice by X-ray diffraction is commonly used and has

investigations, the orientation of the CdTe film is the $(\overline{III})$Te face.[22] We have grown on both CdTe$(\overline{III})$//GaAs(100) and CdTe(100//GaAs(100) substrates and we have seen a difference in the mercury condensation coefficient. This has already been reported for the growth of $Hg_{1-x}Cd_xTe$ films on substrates of different crystallographic orientations.[23] It turns out that growing at 190°C on a (100) orientation requires about 4.4 times more mercury than growing on a $(\overline{III})$Te orientation at the same temperature. But in the (100) orientation no microtwinning due to the formation of antiphase boundaries are observed which makes the growth more easy to control than in the $(\overline{III})$B orientation.

In order to obtain high quality superlattices we use typical growth rates of 3-$Å s^{-1}$ for HgTe and $1Å s^{-1}$ for CdTe. This represents the best compromise between the low growth rate required for high crystal quality, especially for CdTe which should be grown at a higher temperature than 180°C, and the duration of the growth, which should be as short as possible in order to save mercury and to limit the interdiffusion process which cannot be completely neglected between these interfaces (this will be discussed later).

Compared to the growth of HgTe-CdTe SL that of $Hg_{1-x}Cd_xTe$-CdTe SL presents an additional difficulty since we have to control the ternary alloy $Hg_{1-x}Cd_xTe$ instead of the binary compound HgTe. Furthermore, since our goal is the study of the Type III - Type I transition, the composition (x) of the alloy should be very well controlled. In order to have the necessary flexibility for the composition x, a Cd cell plus a CdTe cell or two CdTe cells are required. The growth of $Hg_{1-x}Cd_xTe$ by MBE has already been discussed in numerous papers[24] and the growth of $Hg_{1-x}Cd_xTe$/CdTe SLs successfully achieved.[18]

$Hg_{1-x}Mn_xTe$-CdTe SLs have been grown with x ranging from 0.02 to 0.12 on CdTe$(\overline{III})$//GaAs(100) substrates using three effusion cells containing Hg, Mn and Te for the growth of the alloy and a CdTe cell for the growth of CdTe.[25]

More recently $Hg_{1-x}Zn_xTe$-CdTe SLs have been grown with x ranging from 0.02 to 0.15 on CdTe$(\overline{III})$//GaAs(100) substrates using three effusion cells containing Hg, Te and ZnTe for the growth of the alloy and a CdTe cell for the growth of CdTe.

The proof that these novel superlattice systems have successfully been grown is attested to by X-ray diffraction, as illustrated in Fig. 2. In addition to the Bragg peak one can see satellite peaks due to the new periodicity. The periods of the SLs were measured from the position of the SL satellite peaks as determined by X-ray. The method for determining the period of a superlattice by X-ray diffraction is commonly used and has

been explained elsewhere.[26] The values of the HgTe layer thickness (d_1) 6

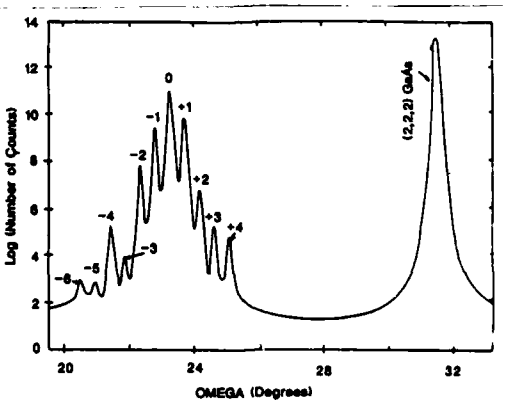

Fig. 2a. Room temperature X-ray diffraction profile about the 222 reflection of a $Hg_{0.92}Cd_{0.08}Te$-CdTe superlattice with a period of 102 Å.

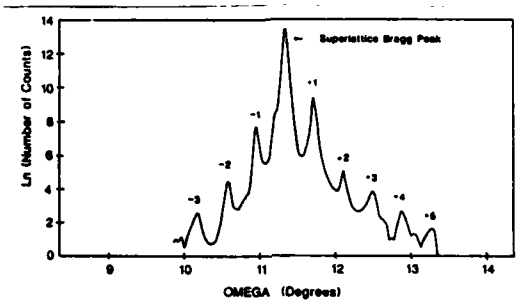

Fig. 2b. Room temperature X-ray diffraction profile about the (111) reflection of a $Hg_{0.87}Mn_{0.13}Te$-CdTe superlattice with a period of 112 Å.

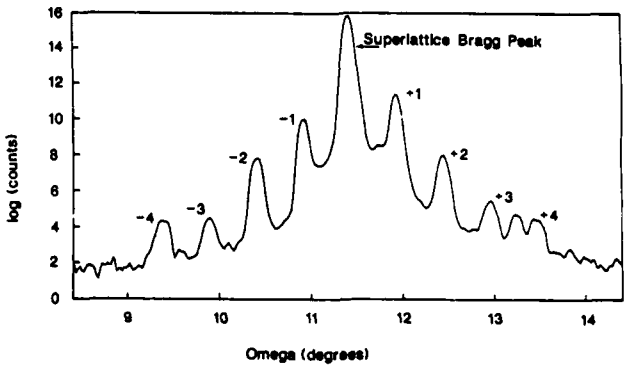

Fig. 2c. Room temperature X-ray diffraction profile about the 111 reflection of a $Hg_{0.99}Zn_{0.01}Te$-CdTe superlattice with a period of 85 Å.

and the CdTe layer thickness (d_2) were then calculated using the Cd and Hg concentrations measured by energy dispersive X-ray analysis (EDAX). In order to prevent the Hg reevaporation from HgTe layers the Hg cell is left open during the growth of CdTe layers. Thus a competition occurs between Hg and Cd. The incorporation of Hg in the CdTe layer depends critically upon several parameters such as the substrate temperature, the crystal orientation and the growth rate. Measurements by secondary ion mass spectroscopy (SIMS), wavelength dispersive spectroscopy (WDS), Raman scattering and EDAX showed that for a thick CdTe film grown under the same condition as we grow our superlattices, there was less than 5% Hg incorporated into the film. Neglecting this small amount of Hg, the ratio of d_2 to the period is just the average Cd composition measured by EDAX. The error in ignoring the Hg in the CdTe and the error in the EDAX measurement itself could lead to errors in d_1 and d_2 of 7 to 8%. Nevertheless, it has been shown recently that more mercury has to be incorporated in the CdTe layers in order to explain the far infrared reflectivity spectra of several superlattices.[27] Thus the question is: does a thick film represent what fraction of Hg is incorporated in a thin film? Experiments are currently carried out in order to answer this question.

III. INTERDIFFUSION

A very important question for the application of this material to optoelectronic device is the thermal stability of the HgTe-CdTe interface. Because of the lower temperature used in MBE compared to other epitaxial techniques such as LPE, OMCVD, or CSVPE, the diffusion processes are more limited in MBE, but the magnitude of this interdiffusion has not yet been fully determined.

To investigate the extent of this interdiffusion, we have carried out temperature-dependent in situ X-ray diffraction measurements on several HgTe-CdTe samples. The estimated interdiffusion constants D(T) are based on the analysis of the X-ray of the nth satellite intensities as a function of time for given temperatures T.

$$\ln \frac{I(t)}{I(t_o)} = -8\left(\frac{\pi n}{L}\right)^2 D(t-t_o)$$ where $L = d_1 + d_2$ is the periodicity of the superlattice.[28] The interdiffusion measurements were carried out using several different techniques to hold and heat the sample. These heating methods called respectively radiative or conductive have been described elsewhere.[29] From the slopes of the intensity of the first-order satellite peak versus time we have calculated the interdiffusion coefficients for five different samples annealed at 185°C which is the usual growth temperature. The results reported in table I show a large

variation for the diffusion constant calculated at 185°C. D for SL 13 is fifty times higher than for SL 54. We think that part of this difference may be due to the experimental method. Nevertheless a difference of about an order of magnitude is observed for different superlattices measured by the same heating technique. The various values obtained from different

Table 1. Results of in-situ interdiffusion measurements on HgTe-CdTe superlattices grown at 185°C in the (III)B orientation

Sample #	# Periods	Period L(Å)	HgTe d_1(Å)	CdTe d_2(Å)	Substrate	Heating method & Environment fordiffusion	Diffusion D(185°C) (cm^2s^{-1})
SL13	250	15	97	60	GaAs	radiative helium	$3.0x10^{-18}$
SL49	142	97	35	62	CdZnTe	radiative helium	$1.8x10^{-18}$
SL52	190	97	36	61	GaAs	radiative helium	$3.0x10^{-19}$
SL54	180	69	44	25	GaAs	conductive mercury	$6.3x10^{-20}$
SL48	170	94	42	52	CdTe	conductive helium	$7.0x10^{-20}$

HgTe-CdTe superlattices to this date emphasize that some material specifications should be assessed before attributing too much importance to the direction of the heat flow through the superlattice. These material specifications can all contribute in many ways to the magnitude of the diffusion coefficients. They are (i) the density of the vacancies; (ii) the content and nature of the impurities; (iii) the density and type of dislocations; (iv) the roughness of the heterojunctions; (v) the quality of the superlattice which can be estimated by the number of satellite peaks observed on each side of the control peak; (vi) the growth rate, which might be related to vacancies, impurities and dislocations; and (vii) the nature of the substrate and that of the buffer layer, as well as the lattice mismatch between these two components of the superlattice.

Furthermore our results indicate that interdiffusion is concentration dependent and thus the interpretations of these results will have to be somewhat modified.

It is important to point out that a diffusion constant D(185) in the range of 3×10^{-18} - $3 \times 10^{19} cm^2 s^{-1}$ is consistent with extrapolation of data obtained by a different group working on the interdiffusion in HgTe-CdTe single junction.[30]

Despite this dispersion in the results it turns out that the thickness of the intermixed layer caused by annealing at the growth temperature of 185°C, calculated from the relation $l = \sqrt{Dt}$, cannot be neglected for thick superlattices required for IR detectors.

Despite these evidences, discussions about interdiffusion during the growth kept on being heard, whether this phenomenon is present or not. In order to answer this question we have grown two thick HgTe-CdTe SLs in the (III)B orientation on GaAs(100) at 185°C. Table II shows the growth data and the period computed from the 1.476Å X-ray data. Three different wavelengths, 0.709Å, 1.282Å and 1.476Å were used to characterize these two SLs. The absorption of the X-rays is used as a tool to probe various

Table 2. Characteristics of HgTe-CdTe superlattices grown on GaAs(100) in the (III)B orientation at 185°C

SL #	# of period	Period (Å)	Duration of growth	Thickness (μm)
SL93	320	198	6h58	6.34
SL95	420	157	8h18	6.60

depths in the SL. Results are similar for both SLs. It is seen (Fig. 3) that the softest wavelength (1.476Å) produces the cleanest and the best diffraction spectrum, emphasizing that the top of the SL has interfaces much sharper than those near the interface with the buffer layer.

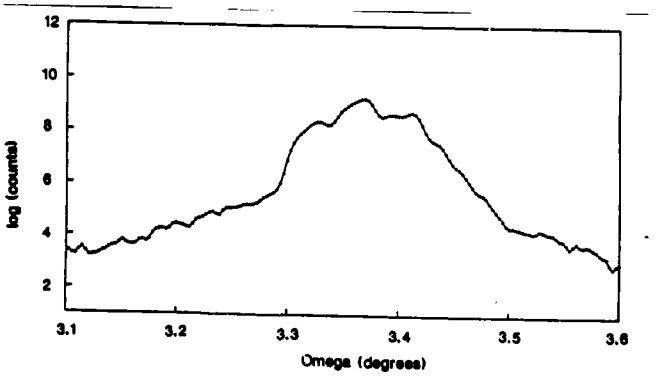

Fig. 3a.

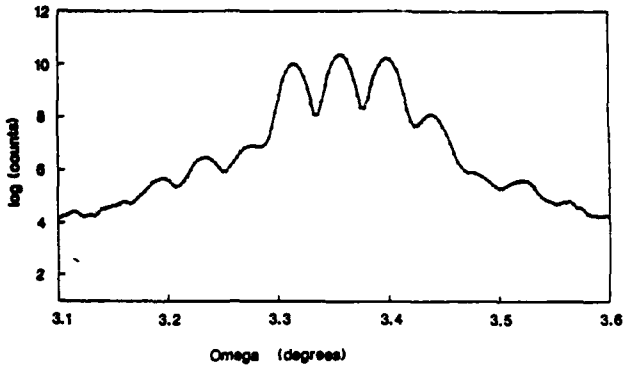

Fig. 3b.

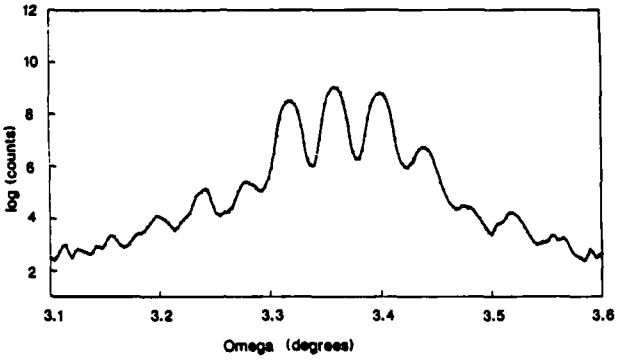

Fig. 3c.

Fig. 3. Room temperature X-ray diffraction profile about the 222 reflection of SL95 X-ray wavelength: (a) 0.709 Å, (b) 1.282 Å, (c) 1.476 Å.

This indeed indicates that significant interdiffusion occurred during the growth of these superlattices in agreement with in situ measurements done on similar superlattices.

In-situ interdiffusion measurements on X-alloyed $Hg_{1-x}X_xTe/CdTe$ superlattices (X = Cd and Mn for this study) reveal that superlattices with x > 0 are more stable than HgTe/CdTe superlattices.[31] These alloyed superlattices have, therefore, a better chemical stability, hence longer device lifetime than the non-alloyed ones, alowing for technological developments to proceed. It is hypothesized that the differences between Fourier components of the diffusion coefficients D(T) are due to Cd- and Mn-substi-

tutions which presumably slow down interstitial and vacancy motions.

IV. SUPERLATTICE BANDGAPS

At low temperature, a precise determination of the SL band gap can be obtained from far-infrared magneto-absorption experiments.[32,33] When a strong magnetic field B is applied perpendicular to the SL layers, the subbands are split into Landau levels. At low temperature (T ~ 4K), the infrared transmission signal, recorded at fixed photon energies as a function of B, presents pronounced minima which correspond to the resonant interband magneto-optical transitions between the valence and conduction Landau levels. The Landau level energies and, therefore, the interband transitions energies, can be calculated in the framework of the envelope function model.[2,34] Good agreement between theory and experiment is obtained for Λ in the range (0-100 meV), taking into account the uncertainties in the sample characteristics. The SL band gap is obtained by extrapolating the energies of the observed transition to B = 0. Figure 4 shows the SL band gap deduced from such experiments in four different samples at 2K. The solid lines in Figure 4 represent the theoretical dependence $E_g(d_1)$ calculated for d_2 = 20, 30 and 50Å using Λ = 40 meV.[35] Experiments and theory are in very satisfying agreement, when Λ is small and positive.

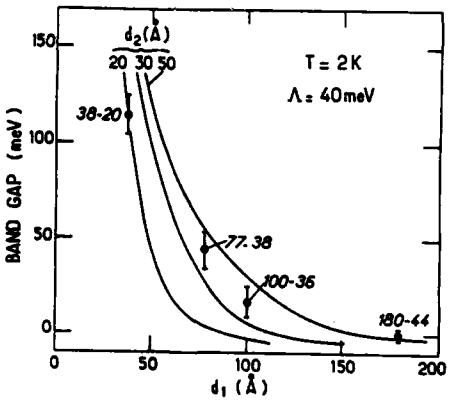

Fig. 4. Variation of the band gap of different hgTe-CdTe superlattices at 2 K as a function of the HgTe layer thickness (d_1). The experimental data are given by the solid dots; for each sample, the first number corresponds to d_1 and the second one to d_2 which is the CdTe layer thickness. The solid lines are theoretical fits for three values of d_2.

In order to determine the SL cutoff wavelength, infrared transmission spectra were measured between 400 and 5000 cm^{-1} at 300K. The absorption coefficient (α) was calculated versus wavelength and the cutoff wavelength was defined to be the wavelength where α is equal to 1000 cm^{-1}. The absorption coefficient was obtained by taking the negative of the natural logarithm of the transmission spectrum and then dividing by the thickness of the SL. Even though the accuracy of this kind of determination is questionable and the value of 1000 cm^{-1} for α is rather arbitrary, we have found that the values of the cutoff determined in this way are in fairly good agreement with those determined by photoconductivity threshold.[36] The bandgap, in eV, is just 1.24 divided by the cutoff wavelength in μm. We do not mean to imply that this technique gives an absolute measure of the bandgap. Rather, it gives a consistent, first order value. The method is quite reproducible (within 5%) and quite simple. It is also quite useful to determine SL's HgTe layer thickness.

We have previously found that this method is not very accurate for thin superlattices.(11) Nevertheless, these investigations confirm that the bandgap of the SL is less than that of the equivalent alloy and that it decreases as the HgTe layer thickness (d_1) is increased, as illustrated in Table 3.

The theoretical value of the SL bandgap is obtained from the SL band structure at $\vec{K} = 0$, calculated using the envelope function approximation.[2,34] The band structures of HgTe and CdTe near the Γ point are described by the 6 x 6 Kane Hamiltonian taking into account Γ_6 and Γ_8 band edges. The interaction with the higher bands is included up to the second order and is described by the Luttinger parameters γ_1, $\gamma_2 = \gamma_3 = \gamma$ (spherical approximation), and K. In this calculation it is assumed that temperature variation of γ_1, γ and K between 4 and 300 K arises essentially from the variation of the interaction gap ϵ_o between the Γ_6 and Γ_8 band edges. For a HgTe-CdTe superlattice, a system of differential equations is established for the multi-components envelope function. The boundary conditions are obtained by writing the continuity of the wave function at the interfaces and by integrating the coupled differential equations across an interface. Taking into account the superlattice periodicity, the dispersion relation of the superlattice is obtained. From this, the superlattice bandgap as a function of the HgTe and CdTe layer thicknesses can be found.[2,32]

Table 3. Characteristics of HgTe-CdTe superlattice grown in the (111) orientation. The superlattice bandgaps are determined from room temperature infrared transmission.

SL#	HgTe (Å)	CdTe (Å)	SL BANDGAP (meV)	COMPOSITION	ALLOY BANDGAP (meV)
1	40	20	155	0.33	335
2	40	60	225	0.60	712
4	74	36	125	0.33	325
5	97	60	100	0.38	401
6	110	48	90	0.30	295
7	86	50	114	0.37	383
8	81	34	113	0.29	281
9	53	34	167	0.39	413
10	47	30	175	0.39	412
11	83	47	117	0.36	374
14	75	31	116	0.29	281
15	58	47	162	0.45	491
16	58	28	135	0.33	325
17	63	37	145	0.37	385
18	36	61	250	0.63	757
19	50	36	180	0.42	452
22	46	48	200	0.51	581
30	107	91	92	0.46	478
31	66	91	144	0.58	684

Figure 5 presents a comparison of the experimental and theoretical bandgaps. The solid lines correspond to the calculated dependence $E_g(d_1)$ for d_2 = 10, 20, 30, 40 and 100 Å at 300K. An offset Δ = 40 meV[35] between the HgTe and CdTe valence band edges is used in these calculations. There is good agreement if one considers the uncertainties in the HgTe and CdTe parameters used in the theoretical calculation and the uncertainties in the experimental determination of the layer thickness. For the SLs with d_2 between 35 Å and 60 Å, an interesting trend can be seen. For the larger values of d_1, the experimental E_g is larger than the theoretical. For the smaller values of d_1, this is just reversed. This suggests some sort of systematic discrepancy between the experimental data and the

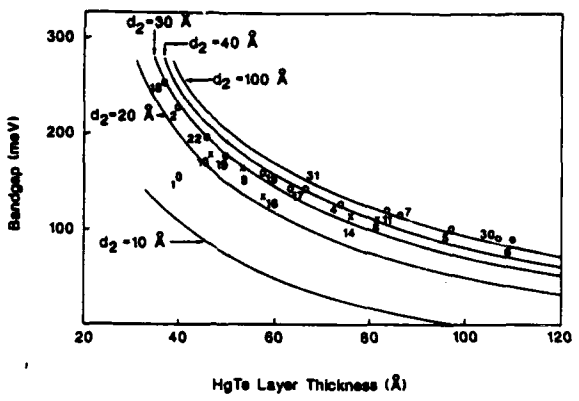

Fig. 5. Variation of the band gap of different HgTe-CdTe superlattices at 300 K as a function of the HgTe layer thickness. The samples characteristics are listed in Table II and the experimental data correspond to the solid circles ($17 \leq d_2 \leq 24$), crosses ($25 \leq d_2 \leq 60$). The solid lines are theoretical fits for different values of the CdTe layer thickness (d_2).

theoretical predictions. A similar discrepancy was seen for bandgaps determined by infrared photoluminescence.[37] For this reason, we believe that this discrepancy between theory and experiment is not due to the experimental technique.

This discrepancy suggests that the experimental data may have a different functional form than the theoretically predicted one. To examine this problem more closely λ_c has been plotted on Fig. 6 as a function of the HgTe layer thickness d_1, for SLs having a CdTe layer thickness (d_2) greater then 40Å, along with the theoretical curve provided by Y. Guldner. Using the technique described above to determine λ_c, we have measured a value of 13.6μm for λ_c of HgTe. We believe that this is the limit of the technique.

A least squares fit was performed on the data to determine the equation of the relationship between λ_c and d_1. Both linear and quadratic terms in d_1 were included in the fit. The coefficient of the quadratic term was found to be 4 orders of magnitude smaller than the coefficient of the linear term. The resulting linear relation was:

$$\lambda_c \text{ (μm)} = 0.1184\ d_1 \text{ (Å)} + 0.78$$

The solid line in Figure 6 corresponds to this equation. If the line is

extrapolated back to $d_1 = 0$, a value of $\lambda_c = 0.78\mu m$ is obtained. The λ_c of CdTe should be about 0.83μm. This is in reasonable agreement with the value obtained by extrapolation of our equation. This linear relation between the cutoff wavelength and the HgTe layer thickness is not predicted by theory as it can be seen in Fig. 6.

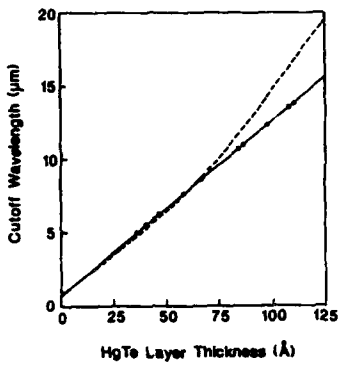

Fig. 6. Cut-off wavelength of HgTe-CdTe superlattices at room temperature as a function of the HgTe layer thickness (d_2 > 40 Å). The experimental data are given by the circles and the solid line is the linear fit. The dotted line is the theoretical curve calculated by Y. Guldner.

Thus we found a difference between theory and experiment in the functional form for the relationship between λ_c and d_1. This is true in spite of the fact that theoretical predictions and experimental measurements give about the same value for the superlattice bandgap. The cause for the discrepancy is not clear at this time.

Infrared photoluminescence of several HgTe-CdTe SLs have been measured as a function of temperature from liquid helium to 300K.[37] The SLs were grown on both GaAs and $Cd_{1-x}Zn_xTe$ substrates with HgTe layer thicknesses ranging from 22Å to 85Å and CdTe layer thicknesses from 18Å to 62Å. Photoluminescence peak positions were observed over the range from 3μm to 17μm (E - 0.4 to 0.07eV). For SLs with HgTe layers 60Å to 85Å thick it is found that the photoluminescence4 peak positions as a function of temperature agree fairly well with the predicted bandgap using a small value (0.04eV) for A.

For superlattices with thinner HgTe layers (22Å to 45Å) the predicted bandgaps were at higher energy than the photoluminescence peak positions.

It is possible to use the cutoff wavelengths determined by IR transmission to go one step further in finding how λ_c depends upon the layer thicknesses.[38] This data can be used to determine an empirical formula for λ_c as a function of both d_1 and d_2. A least squares linear fit has been performed on each of the sets of points with a similar value for d_2. The lines are shown in the Fig. 7. From these fits it is clear that the intercept is approximately constant and is therefore independent of the CdTe layer thickness. But the slope of the lines does depend upon d_2.

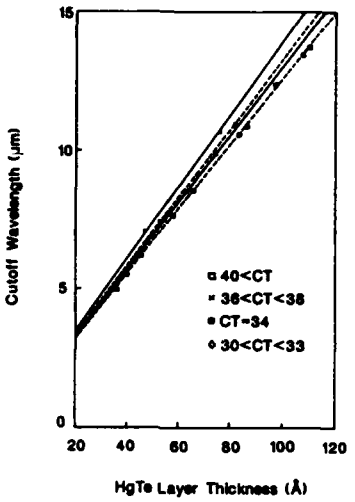

Fig. 7. Variation of the cutoff wavelength of different HgTe-CdTe superlattices at room temperature as a function of the HgTe layer thickness. The data is grouped by CdTe layer thickness. The lines are least squares linear fits of each group of data.

The slopes can then be fit to some functional form. The resulting function of d_1 and d_2 is

$$\lambda_c(\mu m) = [0.3666 \exp(-0.0034 d_2^2) + 0.118]\, d_1 + 0.78$$

V. VALENCE-BAND DISCONTINUITY

The band structure of HgTe-CdTe superlattices have been calculated by using the LCAO or the envelope function models which give very similar results. An important parameter, which determines most of the HgTe-CdTe SL's properties, is the valence band discontinuity Δ between HgTe and CdTe. The value of Δ is presently disputed.

Many models have been recently developed to calculate the band discontinuities. For heterojunctions between compounds having the same anion such as tellurium it has been postulated from the phenomenological "common anion rule"[10] that the valence band discontinuity Δ is small i.e.<0.1eV. This prediction is supported by tight binding calculations.[39] But recent theoretical results, based on the role of interface dipoles do not support the common anion rule and predict a much larger value Δ = 0.5eV.[40] Such a large value has also been calculated recently with a natural lining-up without any dipole contribution: 0.26eV[41] and 0.36eV[42].

The first experimental determination of Δ was obtained from far-infrared magneto-optical experiments at T = 1.6K on a superlattice consisting of 100 periods of HgTe (180Å) - CdTe (44Å). The best agreement between experiment and theory (done in the envelope function approximation) was obtained for Δ = 40 meV.[35]

Since then, additional magneto-absorption experiments have been performed on several other SLs and it has been constantly found that a small positive offset Δ within the limits (0-100meV) provides the best fit.[33]

Resonant Raman Scattering was applied recently to investigate electronic properties of HgTe - CdTe SLs. From these experiments, it has been shown that the Γ_7 holes are confined in the CdTe layers which implies an upper limit of 120 meV for Δ.[43]

As we discussed before, IR photoluminescence measurements agree fairly well with predicted bandgaps using a small value for Δ.

On the other hand, photoemission has been demonstrated to be most valuable for providing direct and microscopic understanding of heterojunction band discontinuities.[44]

Figure 8a illustrates schematically the principle for measuring $\Delta = \Delta E_v$ at the interface between two semiconductors A and B with XPS. If ΔE_v is small ($\lesssim$ 0.5 eV), as for the Te-based heterojunctions, a direct investigation of the valence-band edges, E_v^A and E_v^B, is unrealistic. Indirect measurement involving core levels have to be used. By selecting two core levels, E_c^A and E_{cl}^B, well resolved in energy and by measuring their energy difference ΔE_{cl} across the interface, ΔE_v can be directly deduced according to the following relation [see Fig. 8b].[45,46]

$$\Delta E_v(A\text{-}B) = \Delta E_{cl}(A\text{-}B) + (E_{cl}^A - E_v^A) - (E_{cl}^B - E_v^B) \qquad (1)$$

$E_{cl} - E_v$, the binding-energy (BE) differences between the core level and the top of the valence band for each semiconductor, are determined independently on the bulk semiconductors. All information pertinent to the interface in relation (1) are clearly contained in $\Delta E_{cl}(A\text{-}B)$.

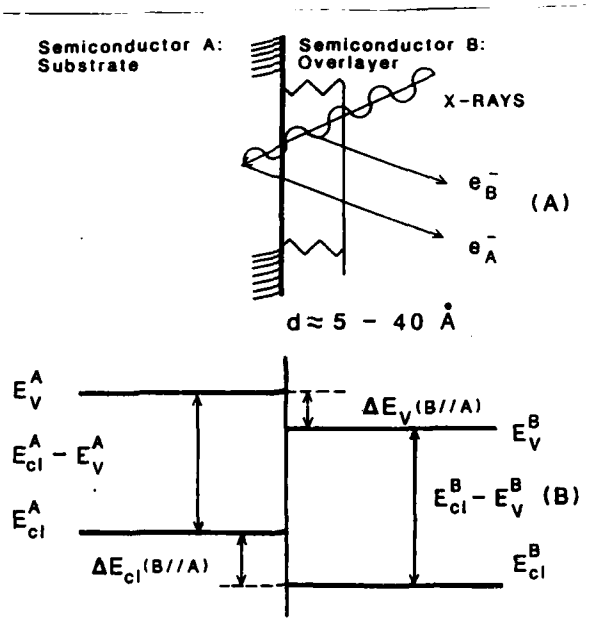

Fig. 8. Principle of determining $\Delta E_v = \Lambda$ with XPS. (a) By irradiating with X-rays semiconductor A covered by overlayer of semiconductor B, XPS spectra of both semiconductors are recorded if overlayer thickness is smaller than electron escape depth. (b) Schematic flat-band energy diagram illustrating relation (1).

Λ was measured recently by XPS and a large value $\Lambda = 0.35$ eV was obtained.[45] This value was determined from a unique sample, grown in one chamber and analyzed in another chamber after exposure to air.

In order to clarify whether there is a discrepancy between optical and XPS data and also in order to verify the commutativity rule not obtained for the GaAs/AlAs system we have performed very careful XPS measurements under well controlled conditions.

The investigated interfaces have been grown in situ by molecular-beam epitaxy with a RIBER 2300 system. Epitaxy came out in the (111) orientation with Te-rich face as controlled by reflection high-energy electron diffraction. Linearity test as well as meaningful comparison with theory requires interfaces to be abrupt at the atomic scale. Thus the growth temperature was maintained at 190°C, a temperature known to give no interdiffusion

across the interface when growth time is short. Moreover, the interface abruptness is inferred from the exponential attenuation with overlayer thickness of the substrate XPS peak.

The samples were directly transferred to the attached spectrometer, at a pressure of 10^{-10} Torr, without transiting through the air. No contamination occurs, avoiding any cleaning procedure. The XPS spectrometer is a SSX-100 model from Surface Science Laboratories using a monochromatized and focussed Al, Kα excitation line. The overall energy resolution measured on $Au_{4f_{7/2}}$ line at a binding energy of 83.93 eV is 0.7 eV. The core levels selected in this work are the resolved spin-orbit components $Cd_{4d_{5/2}}$, $Hg_{5d_{5/2}}$.

The nearly lattice-matched HgTe-CdTe(III)B heterojunctions have been investigated here in great detail. Figure 9 shows the results for ΔE_{cl}, the binding-energy difference between $E_{Cd4d_{5/2}}$ and $E_{Hg5d_{5/2}}$, at different overlayer thicknesses for the two reverse-growth orders. ΔE_{cl} is found to be independent of the overlayer coverage. Meanwhile the Fermi-level position at the interface is varying by 0.2 eV with coverage. This lack of sensitivity of ΔE_v toward interface Fermi-level position, as previously reported for GaAs-Ge,[47] provides the first hint of linearity, in suggesting a ΔE_v "pinning" by the alignment of some reference levels across the heterojunction. Second, ΔE_{cl} is identical for the two growth orders and equal to 2.696 ± 0.030 eV. The experimental uncertaintly is given by the standard deviation, δ, for the measurements.

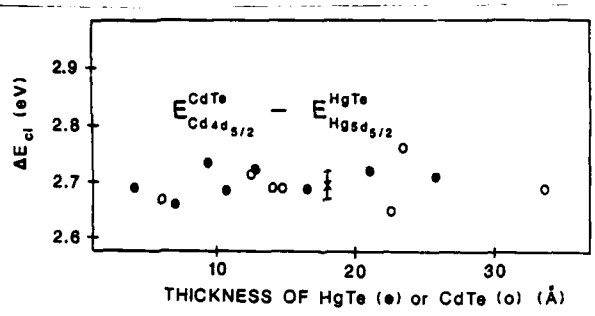

Fig. 9. ΔE_{cl} accross HgTe-CdTe interface as a function of growth order and coverage (open oval, CdTe over HgTe; filled oval HgTe over CdTe).

To obtain $(E_{cl} - E_v)$ used in relation(1), E_v is simply located by linear extrapolation of the valence-band leading edge. This procedure is well justified by the close similarity of the band structure of the tellurides near E_v [see Fig. 10]. It is quite accurate as shown by the δ over numerous

measurements on independent samples: $E^{CdTe}_{Cd4d_{5/2}} - E_v^{CdTe} = 10.145 \pm .030$ eV and $E^{Te}_{Hg5d25/2} - E_v^{HgTe} = 7.805 \pm 0.020$ eV.

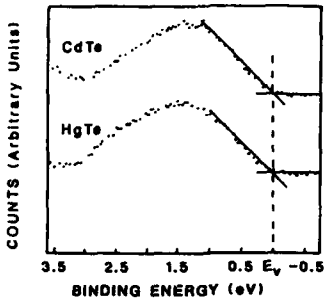

Fig. 10. Linear extrapolation of valence-band leading edge locates the same characteristic feature of the bands taken as E_v. The spectra are shifted to align E_v.

Then $\Delta E_v = \Lambda$ derived for HgTe-CdTe is: 0.36 ± 0.05 eV.[48] This value compares very closely with ref. 45. Hence the discrepancy of XPS with magneto optical data is confirmed but not understood at the present time. Magneto-optical data at 2K as well as the infrared transmission measurements that we have performed at 300K cannot be interpreted by using such a large valence band offset either in the envelope function model or in the LCAO approach. In fact, most of the investigated SLs are calculated to be semimetallic at 4K for $\Lambda = 0.35$eV which is not compatible with the magneto-optical data. It should be pointed out that XPS measurements were carried out at 300K on single and perfectly abrupt heterojunctions whereas magneto-optical, RRS and IR photoluminescence are performed at low temperature on multijunction structures where some interdiffusion cannot be completely ruled out.

In addition, if an appreciable amount of mercury is incorporated during the growth in the CdTe layers that could change the theoretical calculation for Eg and hence the fitting parameter which is precisely the valence band offset.

XPS measurements are currently undertaken in the laboratory on multi-layered structures grown under the same conditions than superlattices in order to shed some light on this discrepancy.

The present center of the theoretical debate on the understanding of Λ is the role played by dipoles at the interface. The core level to valence band maximum binding energy shifts have been measured by XPS for Hg_{1-}

$_xCd_xTe$ alloys.[49] Due to small charge transfer and core level shifts, these shifts are mainly due to valence band maximum shifts. We found that the sum of the valence band shift for HgTe and CdTe in $Hg_{1-x}Cd_xTe$ is constant for the entire range of the alloy composition x and equal to 0.35 eV. This value coincides exactly with the valence band discontinuity measured for HgTe-CdTe heterojunction. Therefore we conclude that there is no need for interface dipole to explain the large valence band offset in agreement with another investigation performed on the alloy $Hg_{0.7}Cd_{0.3}Te$.[50]

VI. TRANSPORT PROPERTIES - TYPE III-TYPE I TRANSITION

One of the most interesting unanswered questions of HgTe-CdTe superlattices is the mobility enhancement in the p-type structures. Hole mobilities have been reported as high as 30,000 $cm^2/V.sec$, but all are above 1,000 $cm^2/V.sec$. Mixing of light and heavy holes has been suggested for the enhancement of the hole mobilities.[17] Several theoretical investigations have been carried out to study this problem. The band structure calculation has been refined using a multi-band tight binding model[51] and the effect of the lattice mismatch between the HgTe and CdTe has been investigated.[51,52] These studies conclude that the light holes should not contribute to the in-plane transport properties.

In order to investigate this interesting problem we have grown related superlattice systems i.e., $Hg_{1-x}Cd_xTe$-CdTe, $Hg_{1-x}Mn_xTe$-CdTe and $Hg_{1-x}Zn_xTe$-CdTe. HgTe-CdTe is called a Type III superlattice because of the inverted band structure of HgTe. In $Hg_{1-x}Cd_xTe$-CdTe SL system at T = 77K when x is smaller than 0.14 it is a type III SL. Whereas, when x is larger than 0.14 it is a Type I SL, similar to GaAs-AlGaAs SL, since HgCdTe is now a semiconductor with both electrons and holes confined in the smaller bandgap material [see Fig. 11].

This Type III - Type I transition is also expected to occur in $Hg_{1-x}Mn_xTe$-CdTe SLs for x ~ 0.07-0.08 and in $Hg_{1-x}Zn_xTe$ - CdTe SLs for x ~ 0.10-0.12 (the effect of the strain has not been taken into account).

Near the transition, strain, valence band offset, alloy disorder, native defects, compensation are the same in Type III and Type I superlattices.

The only difference is the existence of interface states in type III SL but not in Type I SL.

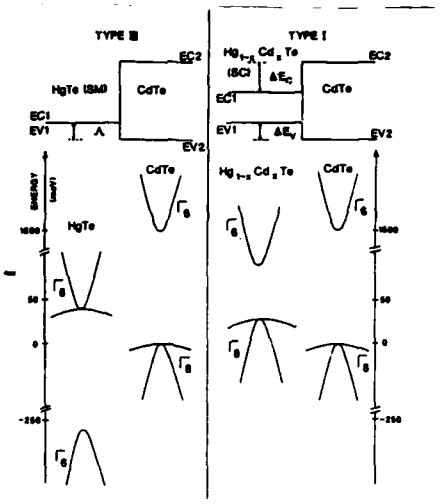

Fig. 11. Band structure of bulk HgTe, CdTe and $Hg_{1-x}Cd_xTe$ illustrating Type III and Type I SL configuration.

In table 4 the Hall characterization of several SL samples is reported. It is interesting to note that if for $Hg_{1-x}Cd_xTe$/CdTe and $Hg_{1-x}Zn_xTe$/CdTe SL systems p type superlattices have been grown none of the $Hg_{1-x}Mn_xTe$-CdTe SLs are p-type. This difference along with the continuous drop of the electron mobility is not currently understood since n and p type $Hg_{1-x}Mn_xTe$ layers have been grown by MBE with high electron hole mobilities.(53)

Table 4 and Fig. 12 show that the hole mobility drops drastically between

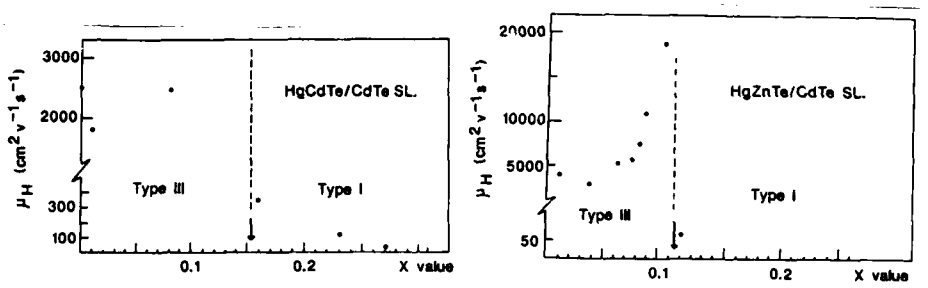

Fig. 12. Hall mobility for holes in $Hg_{1-x}Cd_xTe$-CdTe and $Hg_{1-x}Zn_xTe$-CdTe Type III and Type I SLs.

Type III and Type I. (More $Hg_{1-x}Zn_xTe$-CdTe SLs should be investigated in the Type I region since only one is reported). All these superlattices have been grown in the (111)B orientation on GaAs(100) substrate. It has been previously reported(13) that HgTe-CdTe SLs grown on GaAs exhibit lower

p-type mobilities (μ_H - 10^3-$10^4 cm^2V^{-1}s^{-1}$ range) than those grown on CdTe or CdZnTe (μ_H: 10^4-$10^5 cm^2V^{-1}s^{-1}$ range). If the same tendency is observed for $Hg_{1-x}Cd_xTe$-CdTe SLs it is not the case for $Hg_{1-x}Zn_xTe$-CdTe SLs since a hole mobility as high as 2 x $10^4 cm^2V^{-1}s^{-1}$ is observed for sample #48688. In this system a uniaxial compressional strain which exists in $Hg_{1-x}Zn_xTe$ layers could play a role in the hole mobility by pushing up the light hole band.

In comparison hole mobilities in Type I are in the 10^2-$10^3 cm^2V^{-1}s^{-1}$ range, or even lower, which is the usual range for p type $Hg_{1-x}N_xTe$ alloys. Thus we are dealing with a hole mobility enhancement in Type III SLs and not a hole mobility decrease in Type I SLs. This strongly suggests that the mobility enhancement is related to the presence of the interface states since it is the only change occuring during the transition. It is not surprising that no sudden change in the electron mobility is observed in n-type $Hg_{1-x}Mn_xTe$-CdTe SLs since the interface states involved in the transition have a light hole character and are not supposed to affect the mobility of electrons.

Table 4. Characteristics of $Hg_{1-x}N_xTe$-CdTe (N = Cd, Mn or Zn) superlattices grown at 190°C on CdTe(111)/GaAs(100) substrates. The Hall mobilities were measured at 30K except for sample No. 18124 which was measured at 10K. D_1 = $Hg_{1-x}N_xTe$ layer thickness; D_2 = CdTe layer thickness; n = numbers of periods; x = Cd, Mn or Zn composition in $Hg_{1-x}N_xTe$ layers.

SL System	Type	Sample	x	D_1 (Å)	D_2 (Å)	n	μ_H ($cm^2V^{-1}s^{-1}$)
	III	18124	0	70	45	70	p-$2.5x10^3$
	III	20539	0.01	82	34	120	p-$1.8x10^3$
$Hg_{1-x}Cd_xTe$/	IV	20842	0.08	70	32	100	p-$2.5x10^3$
CdTe	I	20943	0.16	70	40	100	p-$3.5x10^2$
	I	18929	0.23	48	22	90	p-$1.3x10^2$
	I	18728	0.27	69	22	100	p-5 x 10
	III	41880	0.04	168	22	100	n-$2.7x10^4$
	III	42281	0.05	69	26	105	n-$1.5x10^4$
$Hg_{1-x}Mn_xTe$/	III	4169	0.07	86	14	100	n-$5.6x10^3$
CdTe	I	32064	0.09	76	40	150	$n < 10^2$
	I	32266	0.13	66	46	150	$n < 10^2$

	III	47685	0.011	56	29	150	p-4.7x10^3
	III	49092	0.038	109	37	150	p-3.6x10^3
	III	48187	0.064			170	p-5.4x10^3
	III	48789	0.077			150	p-6.0x10^3
$Hg_{1-x}Zn_xTe$/	III	48991	0.082			150	p-7.6x10^3
CdTe	III	47886	0.086			150	p-1.2x10^4
	III	48688	0.103	85	30	150	p-2.0x10^4
	I	46982	0.120			150	p-6 x 10

Hole mobility enhancement has also been observed recently in p-type HgTe-$Hg_{1-x}Cd_xTe$ single heterojunctions[54] where $Hg_{1-x}Cd_xTe$ is a p-type semiconductor. This enhancement was expected since such heterojunction has a Type III interface. The Hall mobility at about 30K of some p-type HgTe-$Hg_{1-x}Cd_xTe$ heterojunctions and $Hg_{1-x}Cd_xTe$ alloys are shown in Table 5. The heterojunctions which contain a thin layer of HgTe between the alloy and the CdTe buffer layer exhibit higher mobilities than the epitaxial layers grown without any HgTe layers.

Table 5. Mobilities of some HgTe-$Hg_{1-x}Cd_xTe$ heterojunctions and $Hg_{1-x}Cd_xTe$ alloys at about 30 K.

Sample	x	d_{HgTe} (Å)	μ_H(cm^2/V sec)
1	0.20	80	1000
2	0.21	60	1000
3	0.20	70	1200
4	0.28	75	1800
5	0.30	85	1100
6	0.33	70	1200
7	0.20	0	560
8	0.25	0	400
9	0.30	0	400

We have made magneto-transport measurements on both Type III SLs and heterojunctions in magnetic fields up to 22 tesla and temperatures as low as 0.5K. Details have been published elsewhere.[55] The observation of the Shubnikov-de Hass oscillations in HgTe-CdTe SL (sample #SLI) and $Hg_{0.92}Cd_{0.08}Te$-CdTe (sample #20842) implies that the hole mobilities are high. We have shown that carriers are in the HgTe or $Hg_{1-x}Cd_xTe$ layers of

the superlattices. Our results determined under identical conditions at 5 tesla are m* = 0.30 and 0.36, respectively, for the two superlattices which are consistent with heavy-hole effective masses in this ternary alloy. Nevertheless, it should be pointed out that the effective mass of holes might be lighter at lower magnetic field where Hall measurements are performed. Indeed, a strong magnetic field dependence has been observed on high hole mobility and from the SL band diagram[33] it can be seen that the curvature of both the heavy hole and interface state bands change much in $\vec{K}$ space.

The Quantized Hall Effect (QHE) has been observed in both Type III p-type superlattices and heterojunctions, confirming the existence of 2D hole gas at the interface.[56] Fig. 13 shows ρ_{xx} and ρ_{xy} for a HgTe-$Hg_{0.72}Cd_{0.28}Te$ heterojunction at 0.5K. The first quantum oscillation for ρ_{xx} is observed at 0.7 tesla. Using the condition $\mu_H B = 10^4$ required for observing quantum oscillation one can deduce that $\mu_H \sim 1.4 \times 10^4 cm^2V^{-1}s^{-1}$ i.e., one order of magnitude larger than what we are measuring by conventional Hall. This is giving credit to the existence of multi carriers in these structures. The same phenomenon has been observed in $Hg_{0.92}Cd_{0.08}Te$ - CdTe SL. Hall measurement indicates a hole mobility of less than $2 \times 10^3 cm^2V^{-1}s^{-1}$ at 0.5 tesla where the first quantum oscillation is observed indicating that μ_H should be equal to $2 \times 10^4 cm^2V^{-1}s^{-1}$ This mixed conduction could explain the apparent difference in hole mobilities between SLs grown directly on CdTe or CdZnTe substrates and those grown on GaAs.

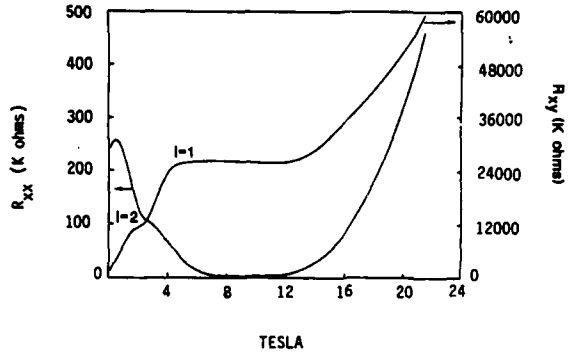

Fig. 13. The ρ_{xx} and ρ_{xy} of a HgTe-$Hg_{0.72}Cd_{0.28}Te$ heterojunction at 0.5 K.

The CdTe buffer layer grown on GaAs could be responsible for this difference. Charge transfer at the CdTe-HgCdTe interface involving deep traps in the CdTe buffer layer has been observed recently.[57]

Concerning the QHE reported in Fig. 13 if the Hall resistance at 2.1

tesla corresponds to i = 2 then i = 1 should be at 4.2 tesla and i = 1/3 should be at 12.6 tesla. We observe the i = 1 Quantized Hall Plateau of about 25.820 ohms between 4 tesla and 13 tesla. Our analysis concluded that these features cannot be explained by sample inhomogeneity but could be explained by a magnetic field dependence of the carrier concentration.[56]

VII. CONCLUSION

In this paper we have reported on very recent developments concerning the growth and the characterization of $Hg_{1-x}Cd_xTe$-CdTe SLs and related Hg based superlattice systems.

These SLs are now currently grown on CdTe, CdZnTe or GaAs substrates. The success of the epitaxial growth on the later substrate represents an important opening due to the high crystal quality of GaAs, its availability in large area and its interest for electronic devices. The only concern with GaAs is its large mismatch with HgTe and CdTe which could generate, even after growth of a buffer layer, some residual strain in the superlattices.

The thermal stability of the HgTe-CdTe interface has been investigated through temperature-dependent in situ X-ray diffraction measurements and, despite the dispersion in the results, it turns out that the interdiffusion cannot be neglected for thick superlattices grown at 185°C. This has been confirmed by probing two thick superlattices grown on GaAs using three different X-ray wavelengths. The softest wavelength produces the cleanest and the best diffraction spectrum emphasizing that the top of the SL has the sharpest interfaces.

A comparison between the experimental room temperature bandgaps and the theoretical predictions from the envelope function approximation has been presented. There is a good agreement when the valence band offset Δ is taken equal to 40 meV. Nevertheless, a systematic discrepancy between the experimental data and the theoretical predictions is observed suggesting that the experimental data may have a different functional form than the theoretically predicted one. We have presented an equation relating λ_c and d_1 for HgTe-CdTe SLs when $d_2 \geq 35$Å. Because the method of determining λ_c is rather simple, this equation makes it possible to determine d_1 quickly and easily as long as d_2 is greater than 35Å. This is very useful to anyone growing HgTe-CdTe superlattices, since in the absence of RHEED oscillations it is difficult to know the layer thicknesses. This linear relation was not predicted by theory. We have proposed an empirical formula for λ_c as a function of both d_1 and d_2

$$\lambda_c(\mu m) = [0.366 \exp(-0.0034\, d_2^2) + 0.118]d_1 + 0.78$$

The value of the valence band discontinuity A is presently disputed both theoretically and experimentally. The phenomenological "common anion rule" postulates that A is small, i.e. < 0.1 eV and this value is supported by magnetooptics, Resonant Raman Scattering, IR photoluminescence and IR transmission experiments. On the other hand, a much larger value of 0.5 eV has been calculated based on the role of interface dipoles. XPS experiments carried out on single heterostructures HgTe/CdTe and CdTe/HgTe agree with a large value of 0.36 eV for A.

But XPS carried out on $Hg_{1-x}Cd_xTe$ alloys have shown that there is no need for interface dipole to explain the large valence band offset. The reason of such a discrepancy in the value of A is still not clear eventhough several hypothesis are currently under investigation.

The Type III - Type I transition has been investigated in p-type $Hg_{1-x}Cd_xTe$-CdTe and $Hg_{1-x}Zn_xTe$-CdTe SLs. It is reported that the hole mobility is drastically enhanced in Type III superlattices but also in Type III heterojunctions. Such mobility enhancement which is not due to modulation doping as in the GaAs-$Ga_{1-x}Al_xAs$ system is attributed to the presence of interface states in Type III structures. A comparison between Hall data and magneto transport measurement concerning the value of the hole mobility indicates that multi carriers could participate to the transport properties in these structures.

The Quantized Hall Effect has been observed in these Type III heterostructures. The large Hall plateau seen between 4 tesla and 13 tesla in a HgTe-$Hg_{0.72}Cd_{0.28}Te$ heterojunction could be explained by a magnetic field dependence of the carrier concentration.

All these recent investigations confirm once again the specific and fascinating character of these novel microstructures.

ACKNOWLEDGMENT

This work is supported by the Defense Advanced Research Projects Agency under Contract No. MDA 903-85K-0030 and the author would like to acknowledge many participants in the Microphysics Laboratory at the University of Illinois at Chicago. J. Reno, I.K. Sou, X. Chu, S. Sivananthan, P.S. Wijewarnasuriya for their assistance in the growth and characterization of the samples, C. Hsu and Tran Minh Duc for their contribution in XPS analysis, S. Rafol and K.C. Woo for performing the magnetotransport experiment.

REFERENCES

(1) J.N. Schulman and T.C. McGill, Appl. Phys. Lett., vol. 34, 663 (1979).

(2) G. Bastard, Phys. Rev., vol. B25, 7584 (1982).

(3) D.L. Smith, T.C. McGill, and J.N. Schulman, Appl. Phys. Lett., vol. 43, 180 (1983).

(4) Y. Guldner, G. Bastard, and M. Voos, J. Appl. Phys., vol. 57, 1403 (1985).

(5) J.P. Faurie, A. Million, and J. Piaguet, Appl. Phys. Lett., vol. 41, 713 (1982).

(6) J.T. Cheung, J. Bajaj, and M. Khoshnevisan, Proc. Infrared Inform. Symp., Detector Speciality, Boulder, CO, 1983.

(7) P.P. Chow and D. Johnson, J. Vac. Sci. Technol., vol. A3, 67 (1985).

(8) K.A. Harris, S. Hwang, D.K. Blanks, J.W. Cook, Jr., J.F. Schetzina, and N. Otsuka, J. Vac. Sci. Technol., A(4), 2081 (1986).

(9) M.L. Wroge, D.J. Leopold, J.M. Ballingall, D.J. Peterman, B.J. Morris, J.G. Broerman, F.A. Ponle, and G.B. Anderson, J. Vac. Sci. Technol., B4, 1306 (1986).

(10) J.O. McCaldin, T.C. McGill, and C.A. Mead, J. Vac. Sci. Technol 13, 802 (1976).

(11) C.E. Jones, T.N. Casselman, J.P. Faurie, S. Perkowitz, and J.N. Schulman, Appl. Phys. Let., vol. 47, 140 (1985).

(12) S.R. Hetzler, J.P. Baukus, A.T. Hunter, J.P. Faurie, P.P. Chow, and T.C. McGill, Appl. Phys. Lett., vol. 47, 260 (1985).

(13) J.P. Faurie, IEEE Journal of Quantum Electronics 22, 1656 (1986).

(14) J. Reno and J.P Faurie, Appl. Phys. Lett. 49, 409 (1986).

(15) L. Esaki, Proc. 17th Int. Conf. Phys. of Semiconductors, Eds. J.D. Chadi and W. A. Harrison. New York: Springer-Verlag, 473 (1985).

(16) Y.C. Chang, J.N. Schulman, G. Bastard, Y. Guildner, and M. Voos, Phys. Rev. B, vol. 31, 2557 (1985).

(17) J.P. Faurie, M. Boukerche, S. Sivananthan, J. Reno and C. Hsu, Superlattices and Microstructures 1, 237 (1985).

(18) J. Reno, I.K. Sou, P.S. Wijewarnasuriya and J.P. Faurie, Appl. Phys. Lett. 48, 1069 (1986).

(19) J.P. Faurie, A. Million, R. Boch and J.L. Tissot, J. Vac. Sci. Technol. A1, 1593 (1983).

(20) J.P. Faurie, J. Reno and M. Boukerche, J. of Cryst. Growth 72, 11 (1985).

(21) J.P. Faurie, C. Hsu, S. Sivananthan and X. Chu - Surface Science 168, 473 (1986), and references therein.

(22) C. Hsu, X. Chu, S. Sivananthan and J.P. Faurie, Appl. Phys. Lett. 48, 908 (1986).

(23) S. Sivananthan, J. Reno, X. Chu and J.P. Faurie, J. Appl. Phys. 60, 1359 (1986).

(24) J.P. Faurie, M. Boukerche, J. Reno, S. Sivananthan and C. Hsu, J.

Vac. Sci. Technol. A3, 55 (1985) (and references therein).

(25) X. Chu, S. Sivananthan and J.P. Faurie, Appl. Phys. Lett. 50, 597 (1987).

(26) D. DeFontaine, Metallurgical Society Conferences, Vol. 36, Edited by J.B. Cohen and J.E. Hilliard, 51 (1966).

(27) S. Perkowitz, D. Rajavel, I.K. Sou, J. Reno, J.P. Faurie, C.E. Jones, T. Casselman, K.A. Harris, J.W. Cook, Jr., and J.F. Schetzina, Appl. Phys. Lett. 49, 806 (1986).

(28) R.M. Fleming, D.B. McWhan, A.C. Gossard, W. Wiegmann, and R.A. Logan, J. Appl. Phys., vol. 51, 357 (1980).

(29) J.-L. Staudenmann, R.D. Horing, R.D. Knox, J.P. Faurie, J. Reno, I.K. Sou, and D.K. Arch, "In-Situ Interdiffusion Measurements in HgTe-CdTe Superlattices," in "Semiconductor Based Heterostructures: Interfacial Structure and Stability," edited by M.L. Green, J.E.E. Baglin, G.Y. Chin, H.W. Deckman, W. Mayo, and D. Narasinham. A Publication of the Metallurgical Society, Inc., Warrendale, PA 15086, 41-57 (1986).

(30) M.F.S. Tang and D.A. Stevenson, J. Vac. Sci. Technol. A5 (1987) (to be published).

(31) J.L. Staudenmann, R.D. Knox and J.P. Faurie, J. Vac. Sci. Technol. A5 (1987) (to be publlished).

(32) Y. Guldner, Proceedings of the International Winter School, Springer-Verlag, 200 (1984).

(33) J.M. Berroir, Y. Guldner, J.P. Vieren, M. Voos and J.P. Faurie, Phys. Rev. B34, 891 (1986).

(34) M. Altarelli, Phys. Rev. B28, 842 (1983).

(35) Y. Guldner, G. Bastard, J.P. Vieren, M. Voos, J.P. Faurie and A. Million, Phys. Rev. Lett. 51, 907 (1983).

(36) M. DeSouza, M. Boukerche and J.P. Faurie (unpublished results).

(37) J.P. Baukus, A.T. Hunter, J.N. Schulman, and J.P. Faurie, J. Vac. Sci. Technol. A5 (1987) (to be published).

(38) J. Reno and J.P. Faurie (to be published).

(39) W.A. Harrison, Phys. Rev. B24, 5835 (1981).

(40) J. Tersoff, Phys. Rev. Lett. 56, 2755 (1986).

(41) C.G. Van de Walle, J. Vac. Sci. Technol. (to be published).

(42) S. Wei and A. Zunger, J. Vac. Sci. Technol. (to be published).

(43) D.J. Olego, P.M. Raccah and J.P. Faurie, Phys. Rev. Lett. 55, 328 (1985).

(44) For recent review, see G. Margaritondo, Solid-State Electron 29, 123 (1986), and references therein.

(45) S.P. Kowalczyk, J.T. Cheung, E.A. Kraut, and R.W. Grant, Phys. Rev. Lett. 56, 1605 (1986).

(46) The notation (B/A) specifies the growth order as B deposited on A and the notation (A-B) is for whatever the growth order is. In addition, the convention adopted regarding the sign of ΔE_v is the following: $\Delta E_v(A-B) > 0$ corresponds to $E_v^B > E_v^A$ in binding-energy scale.

(47) P. Chiaradia, A.D. Katnani, H.W. Sang, Jr., and R.S. Bauer, Phys. Rev. Lett. 52, 1246 (1984).

(48) Tran Minh Duc, C. Hsu and J.P. Faurie, Phys. Rev. Lett. 58, 1127 (1987).

(49) C. Hsu, Tran Minh Duc and J.P. Faurie (to be published).

(50) C.K. Shih and W.E. Spicer, J. Vac. Sci. Technol (to be published).

(51) G.Y. Wu and T.C. McGill, Apl. Phys. Lett. 47, 634 (1985).

(52) J.N. Schulman and Y.C. Chang, Phys. Rev. B33, 2594 (1986).

(53) X. Chu, S. Sivananthan and J.P. Faurie, Appl. Phys. Lett. 50, 599 (1987).

(54) J.P. Faurie, I.K. Sou, P.S. Wijewarnasuriya, S. Rafol and K.C. Woo, Phys. Rev. B34, 6000 (1986).

(55) K.C. Woo, S. Rafol and J.P. Faurie, Phys. Rev. B34, 5996 (1986).

(56) K.C. Woo, S. Rafol and J.P. Faurie, J.Vac. Sci. Technol. (to be published).

(57) Y. Guldner, G.S. Boebinger, M. Voos, J.P. Vieren and J.P. Faurie, Phys. Rev. B (to be published).